Scale-Dependent petrophysical properties in porous media: A pore-network study

by

Misagh Esmaeilpour

B.S., University of Tehran, 2016

A THESIS

submitted in partial fulfillment of the requirements for the degree

MASTER OF SCIENCE

Department of Geology
College of Arts and Sciences

KANSAS STATE UNIVERSITY
Manhattan, Kansas

2021

Approved by:

Major Professor
Behzad Ghanbarian

Copyright

Abstract

Understanding fluid flow and transport in porous media properties has been an active subject of research in the past several decades in hydrology, geosciences and petroleum engineering. However, their scale-dependent characteristics are not yet fully understood. The scale dependence of flow in porous media is attributed to small- and large-scale heterogeneities, such as pore size distribution, pore connectivity, long-range correlations, fractures and faults orientations, and spatial and temporal variations. The main objective of this study is to investigate how permeability (k) and formation factor (F) vary with sample dimension at small scales by means of a combination of pore-network modeling and percolation theory. For this purpose, the permeability and formation factor were simulated in twelve three-dimensional pore networks with different levels of pore-scale heterogeneities. Simulations were carried out at five different network sizes, i.e., 1130, 2250, 3380, 4510 and 6770 μm. Four theoretical models were also developed based on percolation theory to estimate the scale dependence of permeability and formation factor from the pore-throat radius distribution. In addition, two other theoretical scale-dependent permeability models were proposed to estimate the permeability at different scales from the formation factor and/or pore-throat radius distribution. Comparing theoretical estimations with numerical simulations showed that the proposed models estimate the scale dependence of permeability and formation factor accurately. The calculated relative error ranges between -3.7 and 3.8% for the permeability and between 0.21 and 4.04% for the formation factor in the studied pore-networks.

Table of Contents

List of Figures

List of Tables

Chapter 1 - Introduction

Modeling flow and transport in porous media has been an active subject of research in various disciplines, such as groundwater hydrology, petroleum and chemical engineering, civil engineering, soil physics, and geoscience (Ingham and Pop, 2005; Zhao et al., 2019). Since properties of porous media are measured at various scales, e.g., pore, core and reservoir/aquifer, understanding the effect of scale is essential, particularly for relating a property's value at a larger scale (e.g., reservoir) to its value at a smaller one (e.g., core). For this purpose, applying scaling techniques is necessary to transfer knowledge from one scale to another. This can happen by identifying governing mechanisms at smaller scales and then portraying their manifestation at larger scales (Raoof, 2011).

The influence of measurement scale (or sample volume) on physical and hydraulic properties of porous media has been known for decades (Brace, 1984; Ewing et al., 2010; Garbesi et al., 1996; Hyun et al., 2002; Rovey and Cherkauer, 1995; Yoon and Dewers, 2013), and various scaling approaches have been proposed to study the scale dependence of flow and transport in porous media. One of the pioneer models is the Miller-Miller similar-media theory (Miller and Miller, 1956) in which all regions in a porous medium are assumed to be structurally identical magnifications of a reference location. This approach has been widely used to classify porous media based on their hydraulic properties, such as capillary pressure and hydraulic conductivity curves. The Miller-Miller theory is generally valid, as long as media are similar either with respect to their pore space characteristics or their hydraulic properties. Recently, Sadeghi et al. (2016) proposed that the similarity of these properties is not the only required condition. They demonstrated that knowledge of the interrelation between the capillary pressure

and hydraulic conductivity curves quantified within a joint scaling factor is also required for scaling purposes and classifying porous media.

Experimental measurements (Pachepsky et al., 2014; Schulze-Makuch et al., 1999; Tinni et al., 2012) and numerical simulations on rock images (Jing et al., 2016; Wu et al., 2019; Yu et al., 2020) indicate that permeability (i.e., intrinsic permeability), k, increases with the increase in sample volume (or scale). However, beyond a critical volume, interpreted as the minimum scale of an equivalent homogeneous medium (Niemann and Rovey II, 2009), k remains approximately constant. The critical size or volume is known as the representative elementary volume (REV), the smallest sample size above which k does not vary with size (Bear, 1972). Schulze-Makuch et al. (1999) conducted a comprehensive study of scale-dependent permeability by analyzing experimental measurements from 39 different media. They suggested an empirical power-law scaling relationship to correlate the increase in k with the sample volume V_s as follows:

$$k = CV_s^m \tag{1}$$

where the constant C and scaling exponent m characterizing the medium's heterogeneity are empirical. It is not known whether the scaling exponent m in soils depends on the texture (Pachepsky et al., 2014). It has been noted that the structure of media affects the value of m. For example, Schulze-Makuch et al. (1999) found $m = 0.51$ in heterogeneous fractured media and $0.55 < m < 0.83$ in double-porosity media. However, Fallico et al. (2010) reported a substantially smaller value ($m = 0.029$) for a tank filled by sand with a high percentage (76%) of grains between 0.063 and 0.125 mm. Negative exponents, i.e., $m = -0.06$ and -0.05 were also reported in soils (Iversen et al., 2001).

Ghanbarian et al. (2015) applied a machine-learning method called the contrast pattern aided regression (CPXR) and proposed scale-dependent functions to estimate permeability from

other porous media properties using samples from the UNSODA database (Nemes et al., 2001). They showed that by including sample dimensions, i.e., sample internal diameter and height (or length), *k* estimations were substantially improved. However, such functions and the power-law model given in Eq. (1) are purely empirical, and because of their empiricism the interpretation of the parameters (i.e., *C* and *m*) and their variations from one soil/rock sample to another is not clear.

Hopmans et al. (2002) stated that the inherent complexity of flow in heterogeneous media, and the need to integrate theory with experiment, demand innovative and multidisciplinary research efforts to overcome restrictions imposed by current understanding of scale dependence of flow and transport. For example, Hyun et al. (2002) treated a rock as a truncated random fractal and studied the scale dependence of permeability using a stochastic scaling theory.

An explicit theoretical expression for the scale dependence of *k* can be derived in the context of percolation theory (Hunt, 1998, 2001). Hunt (2006) considered an anisotropic medium whose horizontal connectivity was greater than its vertical one and rescaled the medium's axes to have equal conductances in each direction. The transformed medium, accordingly, turned into an isotropic system with elongated volume. Hunt (2006) then combined concepts from percolation theory with the power-law pore-throat size distribution and proposed the following theoretical relationship to characterize the scale dependence of permeability across scales:

$$k(L) = k_{REV}\left[1 - \left(1 - \left(\frac{r_{tmin}}{r_{tmax}}\right)^{3-D_p}\right)\left(\frac{l_{t0}}{l_{t0}+L}\right)^{\frac{1}{\nu}}\right]^{\frac{2}{3-D_p}} \quad (2)$$

where D_p is the pore space fractal dimension characterizing the size distribution of pore throats, k_{REV} is the REV value of permeability, r_{tmin} and r_{tmax} are the minimum and maximum pore-throat

radii in the medium, l_{t0} is the typical pore-throat length, L is the system size, and ν is the correlation length scaling exponent whose universal value is 0.88 in three dimensions (Stauffer and Aharony, 1994). Hunt (2006) set $r_{tmax}/r_{tmin} = 5000$, $D_p = 2.95$, $l_{t0} = 1$, and $k_{REV} = 8.2\times10^{-10}$ m^2 (REV hydraulic conductivity = 0.008 m/s), compared theoretical estimations from Eq. (2) with experimental data from Schulze-Makuch (1996) collected from various sites within a carbonate-rock aquifer in southeastern Wisconsin and found generally good agreement. Results from this comparison are presented in Figure 1.1 where log(K) (K is hydraulic conductivity (m/s)) is plotted against log(V) (V is sample volume (m^3)). In this figure, data are from Schulze-Makuch (1996) and theoretical estimations are from Eq. (2).

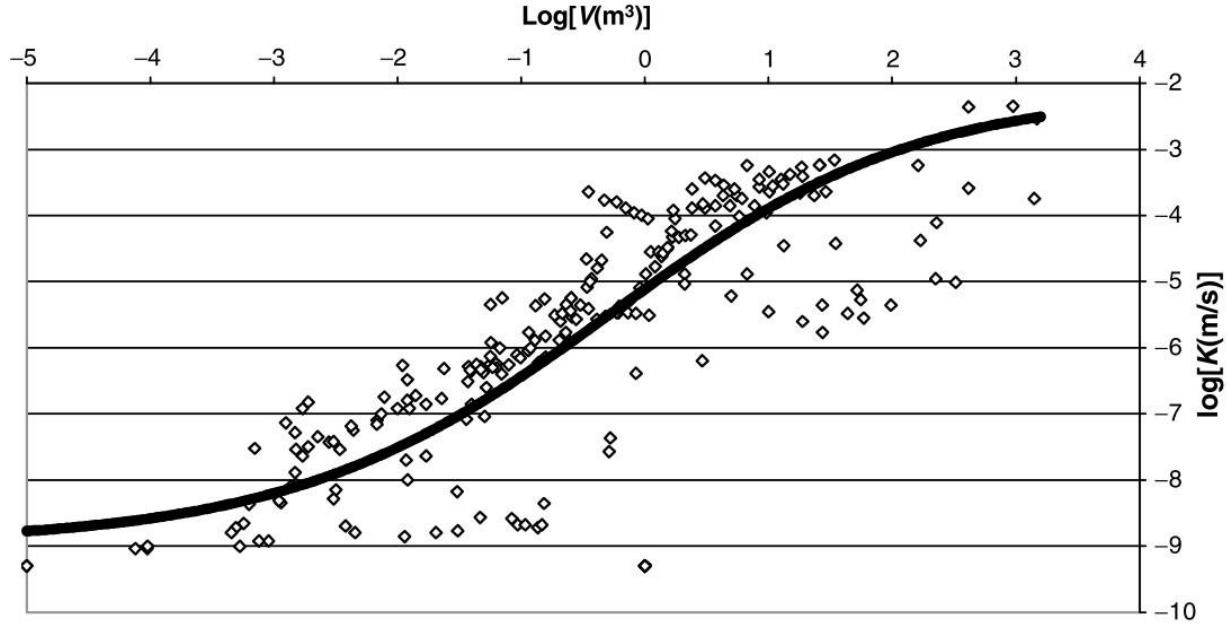

Figure 1.1. Results from Eq. (2) plotted versus the carbonate rock aquifer data from Schulze-Makuch (1996). The black line represents estimations by Eq. (2) and Schulze-Makuch (1996) data are represented as open diamonds (after Hunt, 2006).

More recently, Daigle (2016) combined concepts from the scale dependence of percolation threshold with the permeability model of Katz and Thompson (1986) for fractal

porous media. A similar approach was applied by Davudov and Moghanloo (2017) to study the scale dependence of permeability in shales. However, both models assume that porous media are fractal, and their pore-throat size distributions follow the power-law probability density function.

In the ingenious scale-dependent permeability model of Hunt (2006), Eq. (2), the pore-throat size distribution was approximated by the power-law probability density function. However, lognormal (Cao et al., 2019; Naraghi and Javadpour, 2015), Weibull (Assouline and Selker, 2017; Hidajat et al., 2002), or mixed Gaussian (Cui and Cheng, 2017) distributions may provide more accurate representations in some porous media. There are also some rocks whose pore-throat size distributions do not conform to any type of probability density functions (Cao et al., 2016; Ghanbarian et al., 2020; Saidian and Prasad, 2015; Xu and Prodanović, 2018; Zapata and Sakhaee-Pour, 2016). In addition, Eq. (2) scales down permeability using its REV value, while typically upscaling permeability is desired. In Hunt (2006), Eq. (2) was compared with experimental measurements whose pore space properties were not available. Therefore, the main objectives of this study are to: (1) generalize the Hunt (2006) approach to be independent of the shape of pore-throat size distribution, (2) compare the proposed generalized model with individual pore networks whose pore structures are known, and (3) extend the percolation-based model to formation factor and its scale dependence in porous media.

This thesis is composed of six chapters. An introduction and research objectives are presented in Chapter 1, while Chapter 2 goes into the detail of the methodology of pore-scale simulations (i.e., pore-network modeling). In Chapter 3, we propose theoretical models based on percolation theory and critical path analysis (CPA) for the estimation of permeability and formation factor. Chapter 4 presents the results of pore-scale modeling and theoretical

estimation. Chapters 5 is a brief discussion on accuracy of the models and the research limitations. Finally, Chapter 6 provides concluding remarks and suggestions for future studies.

Chapter 2 - Methodology: Pore-Network Modeling

The primary behavior of multi-phase flow in porous media is controlled by pore-scale characteristics. The information of pore-scale transport processes can be obtained by experimental methods, but they are often time-consuming and expensive. As an alternative, pore-scale modeling can be used to study flow and transport phenomena using information provided at the microscopic pore scale (Raoof, 2011). Pore-network modeling is one of the useful techniques proposed initially back in the 1950s. Fatt (1956) is among those pioneers who applied pore-network models to characterize capillary pressure curve and permeability. Within the pore-network modeling framework, a porous medium can be mapped into a network of pore bodies connected via pore throats (Figure 2.1). This makes it possible to simulate fluid flow directly at the micro scale (Raoof, 2011).

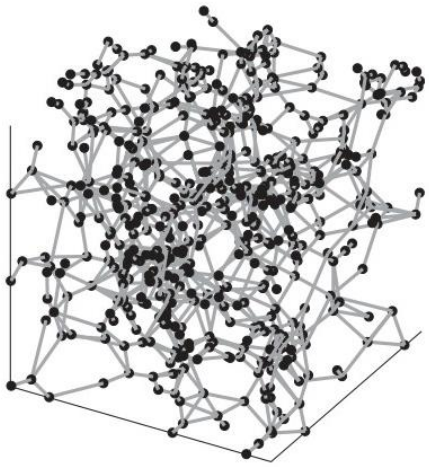

Figure 2.1. A 3D pore-network depicting how pore throats and pore bodies connect to resemble the pore space of a sample (after Valvatne, 2004).

We should point out that in real rocks and soils, the identification of pore bodies, pore throats, and their volumes and sizes is, however, challenging. Blunt (2017) defines pore bodies

as wide regions in the void space of a porous medium and pore throats as narrower regions connecting pore bodies.

Geometry and topology are the two important terms within the PNM (pore-network modeling) framework (De La Garza Martínez, 2016). The former, i.e., geometry, simply represents the number of pore bodies, pore throats, and their size distributions. The latter, i.e., topology, means how pores are connected to each other, typically referred as the pore coordination number indicating the average number of pore throats connected to the same pore body. In real porous media, the pore coordination number is not constant throughout the medium (De La Garza Martínez, 2016) but follows a distribution. There are two types of pore networks: irregular (IPN) and regular (RPN). The difference between these two is that in IPNs there is no pattern for location of pore bodies or pore throats (Figure 2.2). In fact, IPNs can be modelled as though stochastically generated or by directly mapping the exact structure of the sample of interest into a network (Baychev, 2018) (Figure 2.2a). In the latter case, IPN models are sample specific. However, in RPNs the whole network can be divided into cells of the same size, with fixed locations for pore bodies and pore throats that form the skeleton of the model (Figure 2.2b).

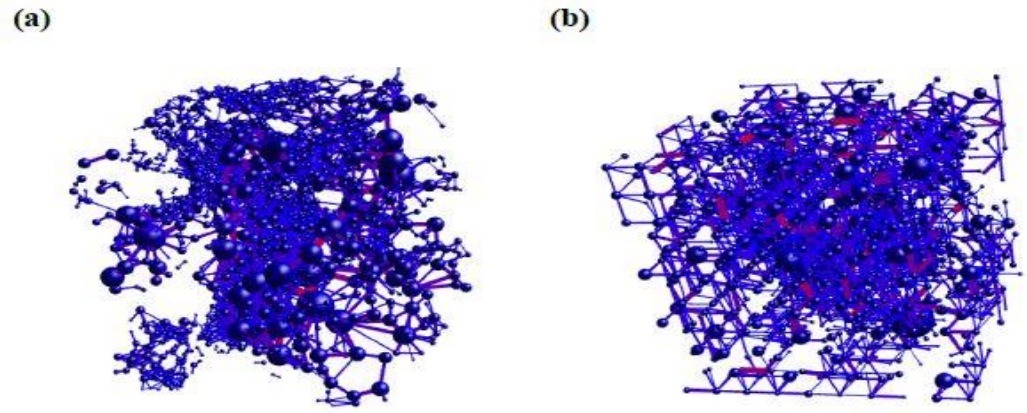

Figure 2.2. (a) Irregular and (b) regular pore network models. Pore bodies are represented by spheres and pore throats by cylinders. Note that the difference between (a) and (b) is the fixed throat length in the latter (after Baychev, 2018).

PNMs can produce reasonably accurate predictions — in a cost-effective manner — for local transport (Valvatne, 2004). Moreover, one can easily modify pore-network model parameters such as geometry, topology, fluid properties, etc. to study their impacts on flow and transport properties (Xiong et al., 2016). Pore-scale modeling is currently a developing research area for determining flow and transport in porous materials (Baychev, 2018; Joekar-Niasar et al., 2012; Mahmoodlu et al., 2020; Zhao et al., 2020). In comparison with other pore-scale modeling methods such as the lattice-Boltzmann method (LBM), PNMs are computationally faster and need less computer resources for execution, which is the reason that more heterogeneity can be added to such models (Xiong et al., 2016).

In this study, we use RPNs constructed by a pore-network generation and fluid flow simulation platform developed by Per Valvatne at Imperial College of London (Valvatne, 2004) to simulate permeability and formation factor in pore-networks of various scales. Regarding the accuracy of this pore-scale modeling platform Valvatne (2004) stated that, "We successfully predicted flow properties for several datasets including a sand pack, a reservoir carbonate and two reservoir sandstones while using a network initially developed to represent Berea sandstone." This suggests that by using this platform we would be able to accurately predict the properties of single and multiphase flow for a broad range of porous media. At the network generation stage, we have control over a number of properties including lattice size (size of network), pore-throat size distribution, pore-body size distribution, pore-throat length distribution, pore geometry, and pore coordination number.

2.1 Pore network generation

To investigate the effect of scale on permeability and formation factor in porous media with different levels of heterogeneity, three different pore-throat radius ranges, i.e., 0.1-10, 1-50

and 10-75 μm were considered. Within each range, four networks were constructed using different values of the Weibull distribution parameters, as described in detail below. Overall, twelve pore networks were generated using the "Netgen" open-access code (written in C++) developed by Valvatne (2004). For this purpose, we generated cubic lattices with fixed coordination number Z = 6 and pore-throat length l_t = 100 μm. Each pore network was composed of cylindrical pore throats and spherical pore bodies.

The size distribution of pore throats conformed to the following truncated Weibull probability density function

$$r_{\mathrm{t}} = (r_{\mathrm{tmax}} - r_{\mathrm{tmin}})(-\delta \ln(x(1 - e^{(1/\delta)}) + e^{(1/\delta)}))^{1/\gamma} + r_{\mathrm{tmin}} \quad (3)$$

where δ and γ are the Weibull distribution shape factors, x is a randomly generated number between 0 and 1, r_t is the pore-throat radius, and r_{tmin} and r_{tmax} are the smallest and largest pore-throat radii, respectively, in the network.

The pore-body radius was accordingly determined based on the following relationship (Valvatne, 2004):

$$r_b = \max\left(\zeta \frac{\sum_{i=1}^{n} r_{ti}}{n}, max(r_{ti})\right) \quad (4)$$

in which n is the number of pore throats connected to the same pore body and ζ is an aspect ratio whose distribution follows the truncated Weibull probability density function. In this study, we set ζ = 0 meaning that the pore-body radius has the same size as the largest connected pore throat.

To generate pore networks of various pore-scale heterogeneities, we used different values of the r_{tmax}/r_{tmin} ratio and Weibull distribution shape factors δ and γ. The summary of properties of all the generated pore-networks is presented in Table 2.1. Using $\delta = 0.2$ results in the pore throat size distribution be left-skewed which is frequently seen in the literature (Ghanbarian et

al., 2020; McPhee et al., 2015; Rahimpour-Bonab and Aliakbardoust, 2014). The parameter γ controls the broadness of the probability density function of r_t and r_b (Figures 2.3a and 2.3b) and thus $12 \leq \gamma \leq 30$ produce a wide range of networks consistent with measurements in real rocks as we show in Chapter 4. To study the scale dependence of permeability and formation factor, we used pore networks of sizes 1130, 2250, 3380, 4510 and 6770 μm, which indicate the length of each side of the pore-network cube.

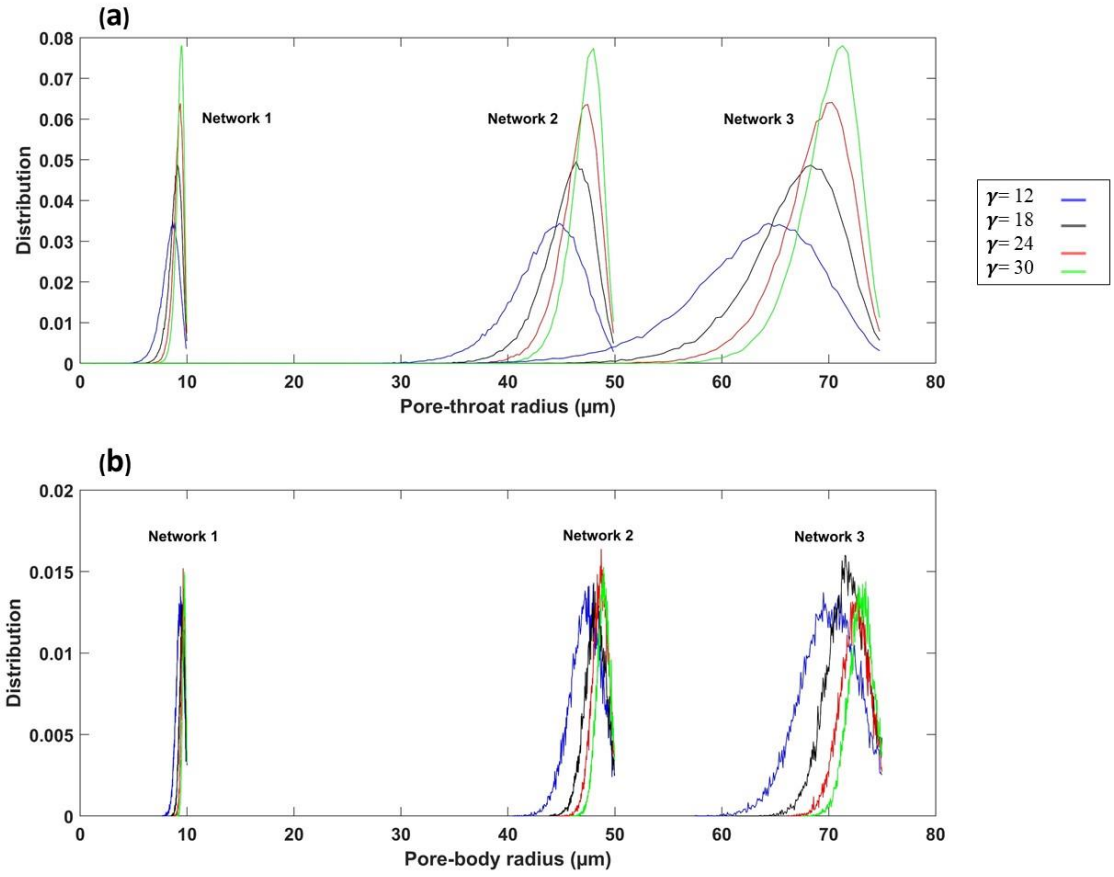

Figure 2.3. Effect of γ value of the Weibull distribution on the (a) pore-throat and (b) pore-body size distribution.

Table 2.1. Salient properties of the twelve pore networks constructed in this study.

Network	r_b (μm)	r_t (μm)	γ	δ	l_t (μm)	Z	r_{tc} (μm)	ϕ (%)
1.1	0.1-10	0.1-10	12	0.2	100	6	8.7	4.3
1.2	0.1-10	0.1-10	18	0.2	100	6	9.1	4.7
1.3	0.1-10	0.1-10	24	0.2	100	6	9.35	4.9
1.4	0.1-10	0.1-10	30	0.2	100	6	9.5	5.1
2.1	1-50	1-50	12	0.2	100	6	44.2	32.1
2.2	1-50	1-50	18	0.2	100	6	46	34.2
2.3	1-50	1-50	24	0.2	100	6	47	35.4
2.4	1-50	1-50	30	0.2	100	6	47.5	36.1
3.1	10-75	10-75	12	0.2	100	6	67.6	43.9
3.2	10-75	10-75	18	0.2	100	6	69.7	46
3.3	10-75	10-75	24	0.2	100	6	70.7	47.1
3.4	10-75	10-75	30	0.2	100	6	71.5	47.8

*r_b is pore-body radius, r_t is pore-throat radius, γ and δ are Weibull distribution parameters, l_t is pore-throat length, Z is pore coordination number, r_{tc} is critical pore-throat radius, and ϕ is porosity.

2.2 Simulating flow in pore networks

Permeability and formation factor were simulated using the "poreflow" pore-scale simulator, also developed by Valvatne (2004). The value of permeability was determined using Darcy's law

$$k = \frac{\mu q_t L}{A_t(P_{inlet} - P_{outlet})} \tag{5}$$

where μ is the fluid viscosity ($Pa.s$), A_t is the medium cross-sectional area (m^2), L is the length (m), q_t is the total flow rate ($\frac{m^3}{s}$), and $P_{inlet} - P_{outlet}$ (Pa) indicates a pressure difference between the inlet and outlet.

The total flow rate was calculated by solving for pressure throughout the network under the steady state flow condition while mass conservation was taking place at each pore body as follows

$$\sum_j q_{ij} = 0 \tag{6}$$

in which i represents each of the pore bodies and j denotes all the pore throats connecting to pore body i. For this equation to be in effect we should suppose that viscous pressure drops are negligible compared to capillary pressure. In Eq. (6), q_{ij} is the flow rate between two pore bodies and depends on the hydraulic conductance g_{hij}, the distance between the centers of the two pore bodies l_{ij}, and the pressure difference ΔP_{ij} as follows

$$q_{ij} = \frac{g_{hij}}{l_{ij}} \Delta P_{ij} \tag{7}$$

The fluid conductance between two pore bodies was determined using the harmonic mean of contributing conductances

$$\frac{l_{ij}}{g_{hij}} = \frac{l_{bi}}{g_{hi}} + \frac{l_t}{g_{ht}} + \frac{l_{bj}}{g_{hj}} \tag{8}$$

in which l_{bi} and l_{bj} indicate the distance in between the center of pore body to the interface where pore body and pore throat meet, and l_t is the pore-throat length (Valvatne, 2004) as shown in Figure 2.4.

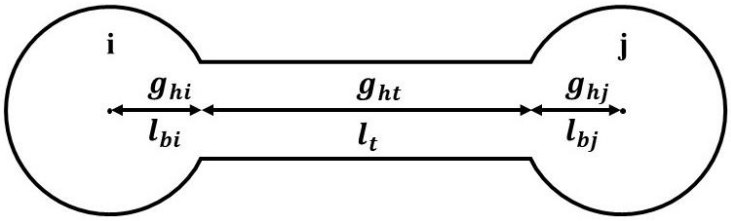

Figure 2.4. Contributing conductances for the calculation of the total conductance between two pore bodies *i* and *j*.

Under laminar flow conditions, the hydraulic conductance is given by

$$g_h = c\frac{A_p^2 G}{\mu} \tag{9}$$

in which *c* is a constant whose value is 0.6, 0.5623 and 0.5 for equilateral triangle, square, and circular pores, respectively, *G* is the shape factor, and A_p is the pore cross section.

Formation factor F in the context of electrical flow is analogous to absolute permeability and hydraulic flow (Valvatne, 2004). It is defined as the ratio of saturated medium resistivity, R_o, to brine resistivity, R_w ($F = R_o/R_w$). R_o can be determined from Ohm's law as follows:

$$R_o = \frac{A_t \Delta V}{a_t L} \tag{10}$$

where ΔV is the change in voltage potential and a_t is the total current flow. Accordingly, the electrical conductance g_e is given by

$$g_e = \frac{A_w}{R_w} \tag{11}$$

where A_w is the cross-sectional area that is occupied by the brine in the pore. From Eq. (11) and Ohms' law we can write (Valvatne, 2004)

$$a_t = g_e \Delta V, \tag{12}$$

then R_o and eventually formation factor F are computed.

Chapter 3 - Theoretical Modeling

Percolation theory from statistical physics provides a theoretic framework to study connections between macroscopic quantities and underlying microscopic properties in homogeneous and heterogeneous networks (Hunt et al., 2014; Sahimi, 1994). Although initial models were proposed based on bond and site percolation classes and regular lattices (Stauffer and Aharony, 1994), more realistic and representative models were developed using irregular and disorder lattices (Kogut and Straley, 1979; Tyč and Halperin, 1989) and the continuum percolation class (Feng et al., 1987; Halperin et al., 1985). In what follows, we apply concepts from percolation theory to generalize the methodology proposed first by Hunt (2006) and establish a general relationship between the critical pore-throat radius and pore space characteristics, such as pore-throat radius distribution and typical pore-throat length as well as the system size.

The fractal nature of clusters — a group of connected sites (pore bodies) and bonds (pore throats) shown in Figure 3.1 — in a percolating system underlies interesting scale-dependent transport modes, e.g., permeability and formation factor (Hunt et al., 2014). Within the percolation theory framework, correlation length gives a measure of the largest length scale at which non-Euclidean or fractal geometry effects are observed. In an infinite system, excluding the percolating (infinite) cluster, the mean distance between any two sites (pore bodies) on the same finite cluster, known as the correlation length χ, is given by (Sahimi, 1994; Stauffer and Aharony, 1994)

$$\chi = \chi_0(p - p_c)^{-\nu}, p > p_c \tag{13}$$

where p is the fraction of bonds or sites that are occupied, p_c is the percolation threshold, ν is the critical scaling exponent whose value is 0.88 in three dimensions (Stauffer and Aharony, 1994),

and χ_0 is the typical bond length (the most frequent bond length). For length scales smaller than the correlation length ($L < \chi$), the system is heterogeneous and statistically self-similar fractal, while for length scales larger than χ the system is macroscopically homogeneous and follows Euclidean geometry (Figure 3.2).

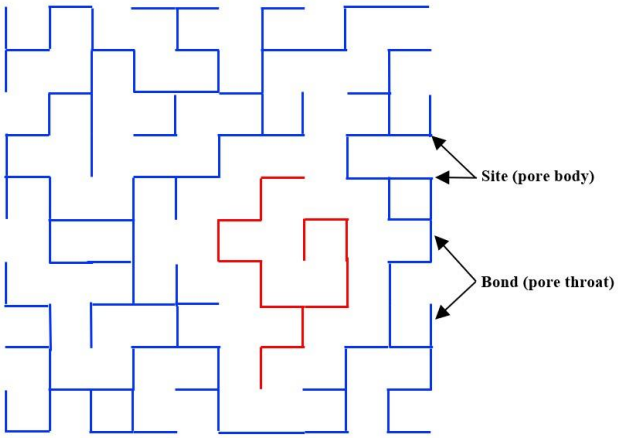

Figure 3.1. Schematic sites and bonds representation of a pore-network. The percolating cluster is shown in blue and the isolated cluster in red.

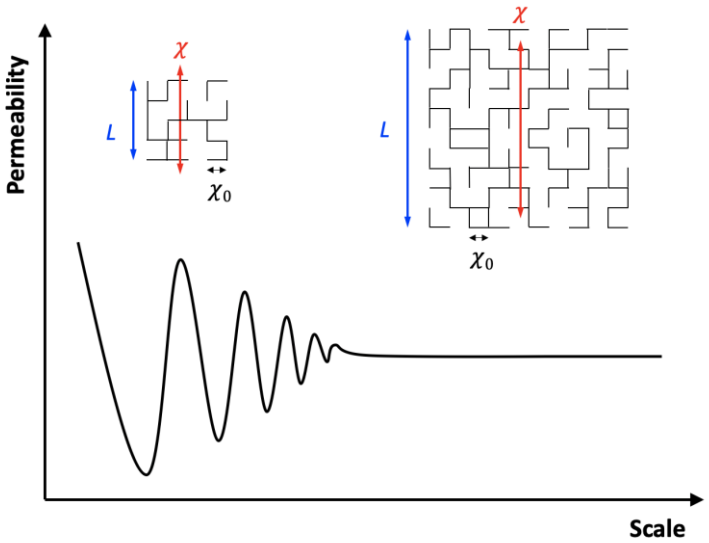

Figure 3.2. The schematic plot of the scale dependence of permeability as well as the representative elementary volume (REV), the smallest size above which permeability does not vary with length. The correlation length, χ, provides a measure of the largest length scale above which the system is macroscopically homogeneous, and the geometry is Euclidean ($L > \chi$). However, when the system size L is less than the correlation length ($L <$

χ), the system is heterogeneous and statistically self-similar fractal. For transport through a system to be truly 3D, all dimensions of the system should be greater than the correlation length χ.

Let us map a porous medium into a network of cylindrical pore tubes. To apply the concept of correlation length from percolation theory to a three-dimensional porous media with irregular pore networks, we need to replace the terms in Eq. (13) for the equivalent terms they have in a pore network. Thus, one may rewrite Eq. (13) as follows

$$\chi = \chi_0 (f - f_c)^{-\nu} \tag{14}$$

in which $f = \frac{V}{V_t}$ is the volume fraction and $f_c = \frac{V_c}{V_t}$ is the critical volume fraction of pores. V represents the occupied pore volume, V_c is the critical volume of pores for percolation, and V_t is the total volume of pores.

Rearranging Eq. (14) gives

$$f = f_c + \left(\frac{\chi_0}{\chi}\right)^{\frac{1}{\nu}} \tag{15}$$

Eq. (15) gives $f = f_c$ for a system of infinite size ($\chi \to \infty$). However, for $\chi < \chi_0$, Eq. (15) returns $f > 1$, which is an unphysical limit. Following Hunt (2006), Eq. (15) can be approximately corrected as follows:

$$f = f_c + \left(\frac{\chi_0}{\chi + \chi_0}\right)^{\frac{1}{\nu}} \tag{16}$$

Such a modification was successfully evaluated by Hunt (2006) to compare scale-dependent permeability estimations with experiments and by Ghanbarian et al. (2013) to estimate scale-dependent tortuosity in porous media.

If $L \to \infty$ it leads to $\chi \to \infty$, accordingly, replacing the typical bond length χ_0 and the correlation length χ respectively with the typical pore-throat length l_{t0} and the system length L in Eq. (16) gives

$$f = fc + \left(\frac{l_{t0}}{L + l_{t0}}\right)^{\frac{1}{v}} \tag{17}$$

In percolation theory, the critical volume of pores V_c can be determined by integrating $l_t r_t^2 f(r_t)$ between r_{tc} and r_{tmax} as follows (Hunt et al., 2014)

$$V_c \propto \int_{r_{tc}}^{r_{tmax}} l_t r_t^2 f(r_t) dr_t \tag{18}$$

where r_t is the pore-throat radius, l_t is the pore-throat length, and $f(r_t)$ represents the pore-throat radius distribution.

Similarly, the total volume of pores is given by

$$V_t \propto \int_{r_{tmin}}^{r_{tmax}} l_t r_t^2 f(r_t) dr_t \tag{19}$$

Accordingly, the critical fractional pore volume can be determined from the ratio V_c/V_t

$$f_c = \frac{V_c}{V_t} = \frac{\int_{r_{tc}}^{r_{tmax}} l_t r_t^2 f(r_t) dr_t}{\int_{r_{tmin}}^{r_{tmax}} l_t r_t^2 f(r_t) dr_t} \tag{20}$$

Following Neuman and his coworkers (Hsieh et al., 1985; Neuman et al., 1984), Hunt (2006) argued that the axes of an anisotropic system can be rescaled to give equal conductances in each direction. Imagine a rectangular system with equal horizontal dimensions but a vertical dimension shorter than the horizontal ones. If the horizontal permeability is 100 times greater than the vertical permeability, the vertical dimension should be 10 times shorter than the horizontal dimensions to have equal conductances in all directions. In such a case, the correlation length would be greater than the horizontal dimension but smaller than the vertical dimension.

However, for transport through a system to be truly 3D, all dimensions of the system should be greater than the correlation length χ. This means that such a transformed medium would be quasi one-dimensional with percolation threshold near 1 (Hunt et al., 2014; Hunt, 2006).

Following Hunt (2006), to determine the scale dependence of the critical pore-throat radius as the critical volume fraction approaches 1 (the fully 1D limit) at small scales, we replace f in Eq. (17) with f_c from Eq. (20) and let $f_c \to 0$ in Eq. (17) to have

$$\frac{\int_{r_{tc}}^{r_{tmax}} l_t r_t^2 f(r_t) dr_t}{\int_{r_{tmin}}^{r_{tmax}} l_t r_t^2 f(r_t) dr_t} = \left(\frac{l_{t0}}{L + l_{t0}}\right)^{\frac{1}{v}} \quad (21)$$

Eq. (21) is the general relationship implicitly linking the critical pore-throat radius to the pore-throat size distribution, typical pore-throat length, and system size. Since r_{tc} in Eq. (21) is not an explicit function of L, we numerically determine its value. Note that, following Hunt (2006), the original f_c in Eq. (17) was set equal to 0 for convenience and simplicity.

In the following, we propose different models based on the relationship between permeability and/or formation factor and the critical pore-throat radius to estimate their scale dependency.

3.1 Estimating the scale dependence of permeability from pore-throat size distribution

A long-standing problem in hydrogeology and petroleum engineering and many other research disciplines has been estimating permeability at a larger scale from its value measured and/or determined at a smaller scale (Hunt, 2003). To address the effect of scale on the permeability, we invoke the critical path analysis (CPA) approach and percolation theory. Katz and Thompson (1986) were first to apply concepts from CPA to estimate permeability from formation factor and critical pore-throat radius in porous media. They proposed

$$k = \frac{r_{tc}^2}{C_{CPA}F} \tag{22}$$

where C_{CPA} is a constant whose value depends on geometrical properties of the pore space (Ghanbarian et al., 2016).

We combine Eq. (21) with Eq. (22), propose two different scale-dependent permeability models, and compare theoretical estimations with pore-network simulations.

Following Hunt (2006), we assume that the critical pore-throat radius varies with the scale via Eq. (21). We further assume that permeability is dominantly controlled by the critical pore-throat radius as suggested in Eq. (22). Accordingly, we set $k(L) \propto r_{tc}^2(L)$ and normalize permeability using its value at the smallest scale L_{min} (i.e., L = 1130 μm) as follows

$$k(L) = k(L_{min}) \left[\frac{r_{tc}(L)}{r_{tc}(L_{min})}\right]^2 \tag{23}$$

Recall that $r_{tc}(L)$ can be numerically computed by solving Eq. (21) given that $f(r_t)$, l_{t0}, and L are known for the pore networks studied here. Following Katz and Thompson (1986), we determine the value of $r_{tc}(L_{min})$ from the mode of the pore-throat size distribution (see Table 2.1).

The power-law relationship between k and r_{tc} may not follow the quadratic relationship given in Eq. (23). Reanalyzing experimental data reported by Katz and Thompson (1986) revealed an exponent equal to 2.36 (Figure D.1 in Appendix D). Ghanbarian et al. (2017) also found an exponent less than 2 (i.e., 1.90). We accordingly generalize Eq. (23) to have

$$k(L) = k(L_{min}) \left[\frac{r_{tc}(L)}{r_{tc}(L_{min})}\right]^{\alpha} \tag{24}$$

where the value of α can be determined from the simulations by fitting a power law to the permeability values simulated at L = 1130 μm versus the critical pore-throat radius derived from the mode of the pore-throat radius distributions.

3.2 Estimating the scale dependence of formation factor from pore-throat size distribution

Formation factor F is another important porous medium's property that has been widely investigated (Adler et al., 1992; Ghanbarian and Male, 2021; Moradllo et al., 2018; Revil et al., 2015). However, the theoretical modeling of its scale dependence has remained as an open question in the literature. In the following, we propose two scale-dependent F models using the CPA approach and percolation theory.

Following Ewing and Hunt (2006), one may invoke concepts from CPA to establish a theoretical relationship between the formation factor and the critical pore-throat radius, i.e., $F \propto r_{tc}^{-1}$. Applying this relationship in combination with Eq. (17) provides the following scale-dependent F model

$$F(L) = F(L_{min}) \left[\frac{r_{tc}(L)}{r_{tc}(L_{min})}\right]^{-1} \tag{25}$$

Similar to the scale-dependent permeability, the relationship between F and r_{tc} may not conform to an inverse linear equation and Eq. (25). Reanalyzing experimental measurements reported by Katz and Thompson (1986) revealed an exponent equal to -0.44 (Figure D.2 in Appendix D). We, therefore, propose the following model for the scale dependence of the formation factor

$$F(L) = F(L_{min}) \left[\frac{r_{tc}(L)}{r_{tc}(L_{min})}\right]^{-\beta} \tag{26}$$

in which the value of the exponent β can be determined from the simulations and by directly fitting a power law to the formation factors plotted against their corresponding r_{tc} values.

3.3 Estimating the scale dependence of permeability from formation factor and/or pore-throat size distribution

In the Hunt (2006) model, it is assumed that the value of critical pore-throat radius varies with the scale. In this section, we propose two other models based on the Katz and Thompson (1986) relationship, Eq. (22), to estimate $k(L)$ from either $F(L)$ or pore-throat radius distribution and formation factor.

If pore-throat radius distribution does not significantly change with scale, one may assume that permeability is dominantly controlled by formation factor and set $k(L) \propto 1/F(L)$. Accordingly, normalizing permeability using its value at the smallest scale gives

$$k(L) = k(L_{min}) \frac{F(L_{min})}{F(L)} \tag{27}$$

Eq. (27) provides a simple relationship to determine the scale dependence of permeability from permeability measured/simulated at the smallest scale, $k(L_{\min})$, and the formation factor measured/simulated at both scales. Although such a linear proportionality is valid in pore-network simulations where pore-throat radius distributions do not change from one scale to another, it may not be held in real rocks (Ghanbarian and Male, 2021).

If the value of $k(L_{\min})$ is not available, one may estimate it via the Katz and Thompson (1986) model, Eq. (22). Combining Eq. (27) with Eq. (22) yields

$$k(L) = \frac{r_{tc}^2(L_{min})}{C_{CPA} F(L)} \tag{28}$$

To estimate the scale dependence of permeability via Eq. (28), one needs the formation factor measured/simulated at that scale and the critical pore-throat radius at the smallest scale.

The latter can be determined from the pore-throat radius distribution. In this study, we set C_{CPA} = 32, following Friedman and Seaton (1998).

3.4 Model evaluation criteria

To evaluate the accuracy of the proposed scale-dependent models, the root mean square log-transformed error (RMSLE) and the relative error (RE) values were calculated as follows

$$RMSLE = \sqrt{\frac{1}{N}\sum_{i=1}^{N}[\log(x_{\text{est}}) - \log(x_{\text{sim}})]^2} \tag{29}$$

$$RE = \frac{x_{\text{est}} - x_{\text{sim}}}{x_{\text{sim}}} \times 100 \tag{30}$$

where N is the number of samples, and x_{est} and x_{sim} are, respectively, the estimated and simulated values.

Chapter 4 - Results

In this section, we present the results of comparing the pore-scale numerical simulations with the proposed theoretical models from percolation theory. According to experimental evidence, Nelson (1994) classifies a few types of media, based on their $k - \phi$ trends shown in Figure 4.1a on semi-log scale. As can be seen, pore networks studied here represent unconsolidated sands (Network 2 and 3) and/or consolidated sands and carbonates (Network 1). Figure 4.1b shows that the $k - \phi$ trend in our simulations are in well agreement with experiments from the literature. Figure 4.2 shows the pore-throat radius distributions for all twelve pore networks studied here. As can be seen from Figure 4.2 (also indicated in Table 2.1), Networks 1, 2, and 3 have three distinct ranges of pore-throat radii to study the scale dependence of permeability and formation factor in porous media of different levels of heterogeneity. Network 1 has the narrowest pore-throat radius distribution among all the networks (Figure. 4.2) and represents the most homogeneous medium, while Networks 2 and 3 represent respectively the intermediate and the most heterogeneous media in this study. We should also point out that as the parameter γ in the Weibull distribution, Eq. (3), increases (Figure 2.3), the average value of r_t increases as well. However, the pore-throat radius distribution becomes narrower (Figure 2.3 and Figure. 4.2). Accordingly, the level of heterogeneity decreases from Networks 1.1, 2.1, and 3.1 to Networks 1.4, 2.4, and 3.4.

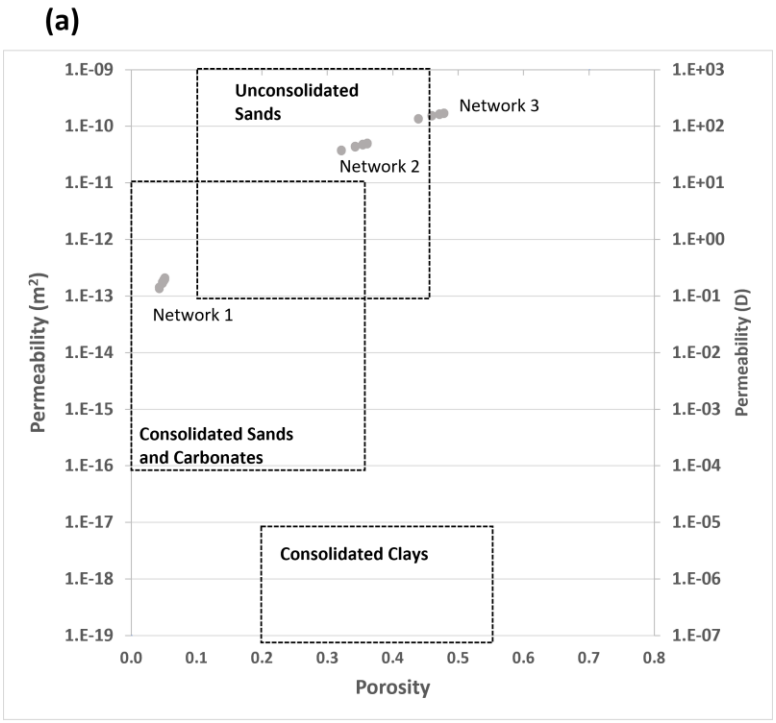

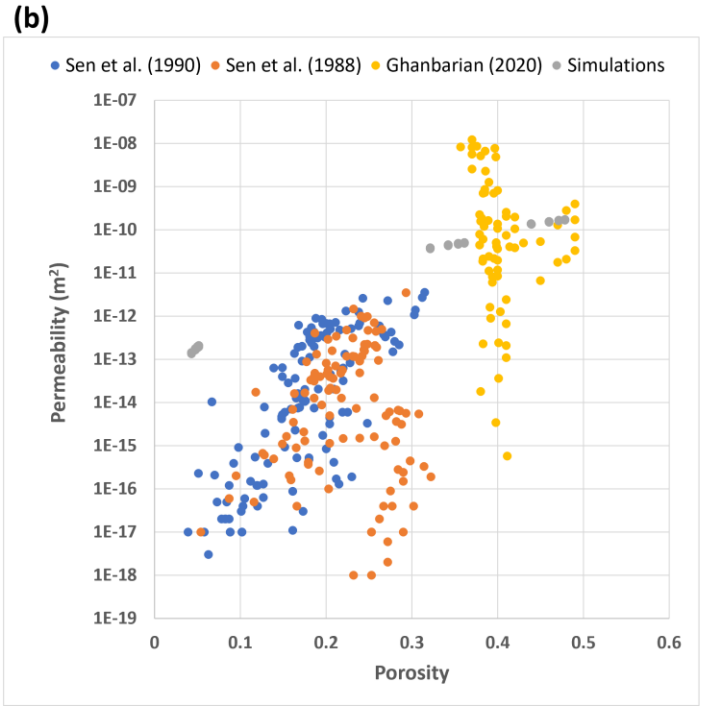

Figure 4.1 (a) Reproduced figure from Nelson, (1994). Simulation values are indicated by gray filled circles. (b) k-ϕ plot of simulation results and experimental data from literature (Ghanbarian, 2020; Sen et al., 1990, 1988).

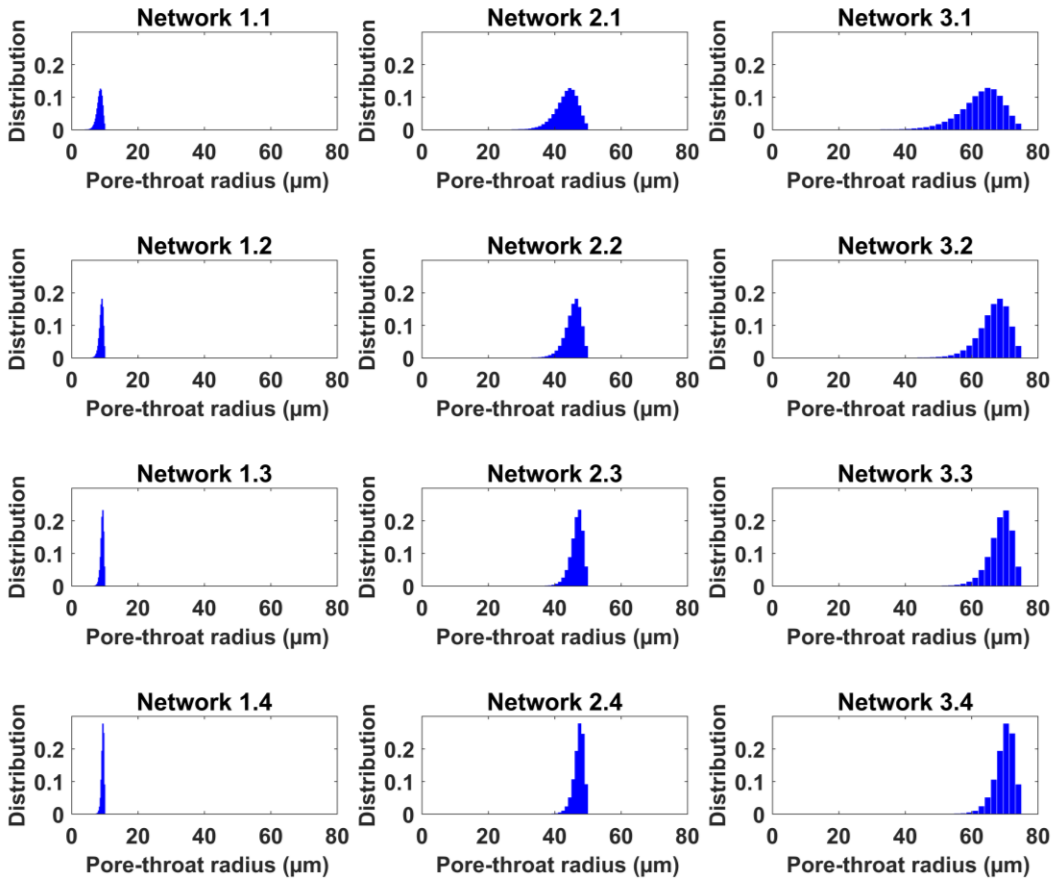

Figure 4.2. Pore-throat radius distributions for the twelve pore networks constructed in this study.

The pore-body radius distributions of all the networks are presented in Figure. 4.3. Since we set $\zeta = 0$ in Eq. (4), the pore-body radius has the same size as the largest connected pore throat. As a result, the pore-body radius distributions of the networks resembled probability density functions similar to the pore-throat radius distributions.

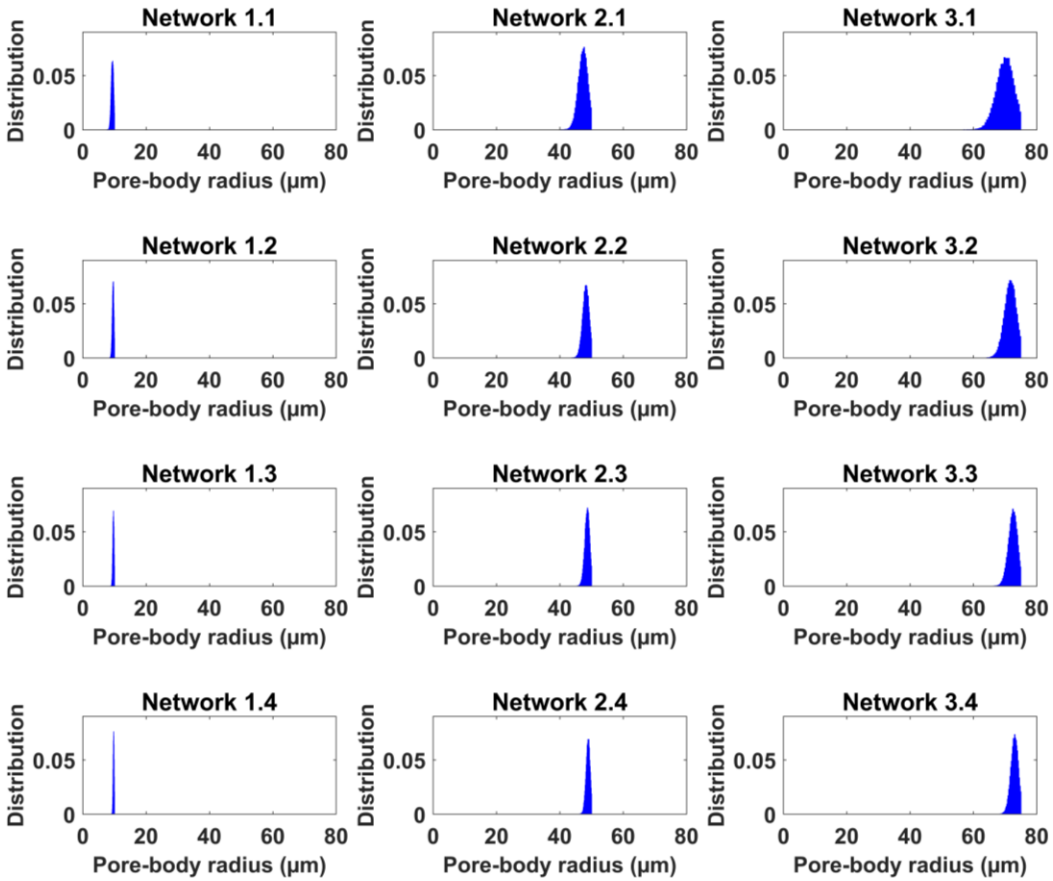

Figure 4.3. Pore-body radius distributions for the twelve pore networks constructed in this study.

To determine the exponents α in Eq. (24) and β in Eq. (26), we plotted the permeability and formation factor values simulated at the smallest network with L = 1130 μm versus the critical pore-throat radius and fitted the power-law function to the data. Results shown in Figure 4.4 indicate that α = 3.03 and β = 1.37 with $R^2 > 0.94$. We reanalyzed the experimental data from Katz and Thompson (1987) and numerical simulations from Berg (2014) and found α = 2.36 and 4.71 and β = 0.44 and 2.66, respectively (Figures D.1- D.4 in Appendix D). Our α = 3.03 and β = 1.37 are in accord with the range obtained from the literature. β = 1.37 in Eq. (26), is not greatly different from the exponent -1 in Eq. (25). Accordingly, the scale-dependent

formation factor estimations by these two equations should not be substantially different, as we show in what follows. For permeability, α = 3.03 in Eq. (24), however, is greater, by a factor of 1.5, than the exponent 2 in Eq. (23).

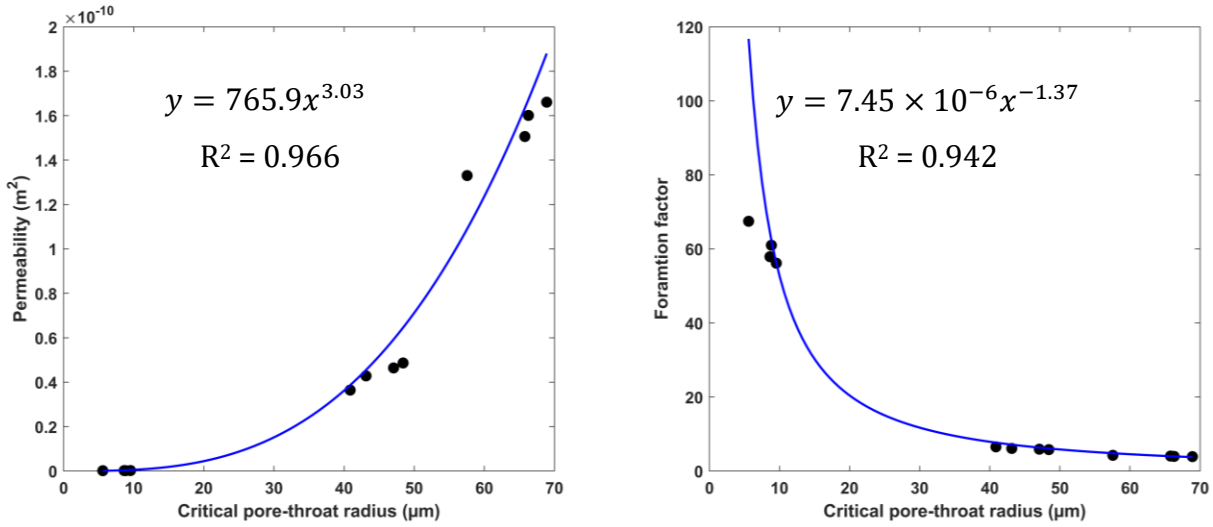

Figure 4.4. Permeability (left) and formation factor (right) versus critical pore-throat radius. Blue lines are the best power-law function fitted to the simulations. Both permeability and formation factor simulations are from the smallest network with *L* = 1130 μm. The critical pore-throat radius was determined from the mode of the pore-throat radius distribution that does not vary with network size.

4.1 The scale dependence of porosity in pore networks

We determined the porosity for each of the twelve pore networks studied here. From Network 1 to Network 3 as the pore-throat and pore-body radius distributions become broader and their mean values greater, an increase in porosity is expected as shown in Figure 4.5. Furthermore, for networks with the same r_{tmin} and r_{tmax} values (i.e., Network 1.1 to 1.4, Network 2.1 to 2.4, and Network 3.1 to 3.4) since increasing the parameter γ in the Weibull distribution results in an increase in the mean value of r_t and r_b, higher porosities are expected for networks with greater γ values. Since pore-throat and pore-body radius distribution, and coordination number do not statistically vary with scale within our networks, we do not expect to

see much variation in the simulated porosity values with network size (Figure 4.5). However, the scale dependence of porosity may change for networks of sizes smaller than 1130 μm or greater than 6670 μm. This would be consistent with results of Yoon and Dewers (2013) and Aslannejad et al. (2017) who found that the value of porosity can change with scale.

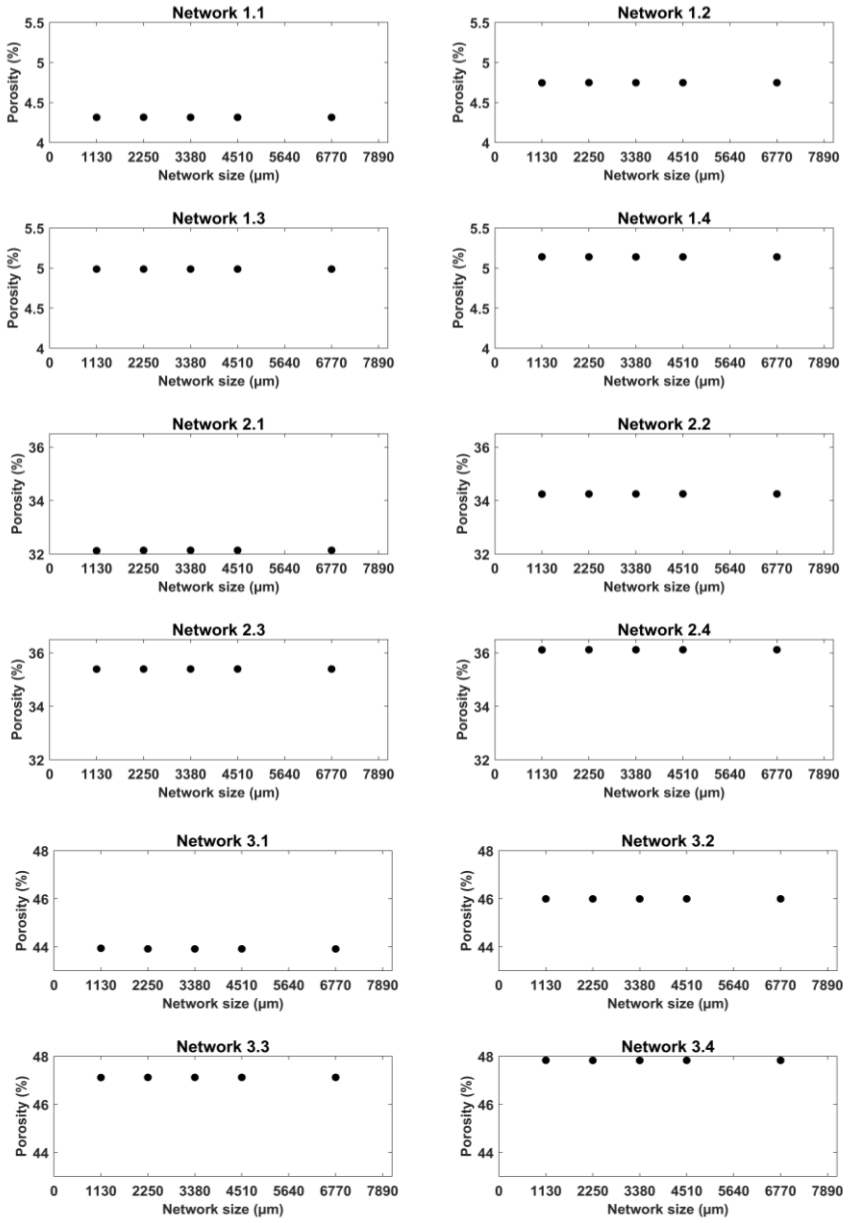

Figure 4.5. Simulated porosities for the twelve pore-networks studied.

4.2. Estimating the scale dependency of permeability and formation factor from pore-throat radius distribution

4.2.1 Network 1

Figure 4.6 presents the results of pore-scale numerical simulations of k and F and the theoretical estimations by the proposed models, Eqs. (23)-(26). As reported in Table 2.1, the value of r_{tc} increases from Network 1.1 to 1.4. Therefore, based on the CPA and Eq. (22) one should expect the value of permeability to increase from Network 1.1 to 1.4 as well, as shown in Figure 4.6. Using the same terminology and given that the relationship between F and r_{tc} is inverse, one should expect the value of the formation factor to decrease from Network 1.1 to 1.4.

Figure 4.6 also shows that the simulated permeability increases with increase in the network size, although the pore-throat radius distribution does not statistically vary with the scale. The theoretical estimations of the scale-dependent permeability are also presented in Figure 4.6, and the corresponding RMSLE value for each model is also reported. For the permeability, the RMSLE value ranged from 0.0075 to 0.0187, and 0.0032 to 0.0156 for the estimations based on Eq. (23), and Eq. (24), respectively. For the formation factor, we found $0.0141 < \text{RMSLE} < 0.0194$ for Eq. (25) and $0.0112 < \text{RMSLE} < 0.0185$ for Eq. (26), as reported in Figure 4.6.

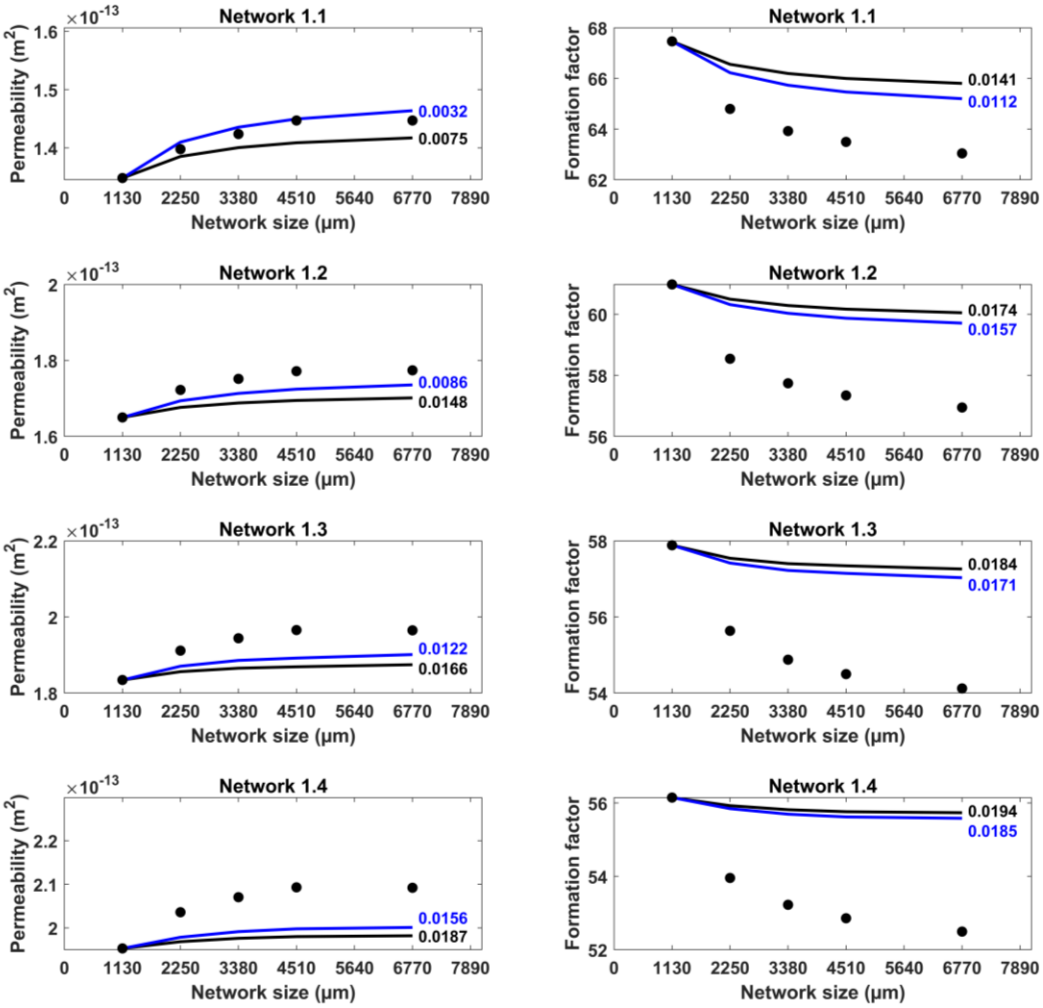

Figure 4.6. Simulated and estimated permeability and formation factor for Network 1. Black filled circles indicate simulation values. Black and blue lines represent estimations by Eqs. (23) and (24) for the permeability and by Eqs. (25) and (26) for the formation factor, respectively. The calculated RMSLE value for each model is given adjacent to each line using the same color code.

We also report the values of relative error (RE) and relative absolute error (RAE) as well as their averages in Table 4.1. It is clear from Figure 4.6 that Eq. (23) and Eq. (24) underestimates the scale-dependent permeability. This is confirmed via the negative RE values reported in Table 4.1. Results from Network 1 show that Eq. (24) with average RE = -1.67% estimates $k(L)$ more accurately than Eq. (23) with average RE = -2.85%. For the formation

factor, both models overestimate the scale-dependent F in the studied networks. However, Eq. (26) with average RE = 3.24% estimates $F(L)$ slightly more accurately than Eq. (25) with average RE = 3.6% (Table 4.1).

Table 4.1. Calculated values of relative error (RE) and relative absolute error (RAE) for theoretical models developed to estimate the scale dependence of permeability and formation factor in twelve pore networks using Eq. (23), Eq. (24), Eq. (25), and Eq. (26).

Pore network	Permeability k				Formation factor F			
	Eq. (23)		Eq. (24)		Eq. (25)		Eq. (26)	
	RE	RAE	RE	RAE	RE	RAE	RE	RAE
1.1	-1.45	1.45	0.61	0.61	2.92	2.92	2.31	2.31
1.2	-2.95	2.95	-1.74	1.74	3.62	3.62	3.25	3.25
1.3	-3.29	3.29	-2.43	2.43	3.81	3.81	3.54	3.54
1.4	-3.70	3.70	-3.10	3.10	4.04	4.04	3.85	3.85
Average	-2.85	2.85	-1.67	1.97	3.60	3.60	3.24	3.24
2.1	-0.45	0.45	1.26	1.26	1.68	1.68	1.19	1.19
2.2	-1.36	1.36	-0.28	0.28	2.10	2.10	1.78	1.78
2.3	-1.81	1.81	-1.10	1.10	2.32	2.32	2.11	2.11
2.4	-2.07	2.07	-1.54	1.54	2.44	2.44	2.29	2.29
Average	-1.42	1.42	-0.42	1.05	2.14	2.14	1.84	1.84
3.1	0.74	0.74	2.86	2.86	0.80	0.80	0.21	0.21
3.2	-0.46	0.46	0.84	0.84	1.36	1.36	0.98	0.98
3.3	-1.11	1.11	-0.27	0.27	1.68	1.68	1.43	1.43
3.4	-1.30	1.30	-0.64	0.64	1.77	1.77	1.57	1.57
Average	-0.53	0.90	0.70	1.15	1.40	1.40	1.05	1.05
Overall average	-1.60	1.72	-0.46	1.39	2.38	2.38	2.04	2.04

*values are in percentage

Comparing the scale-dependent permeability and formation factor estimations shown in Figure 4.6, it appears that the scale dependence of permeability is more closely estimated than that of formation factor. This may be because the hydraulic conductance of a cylindrical pore is proportional to its radius to the fourth power, while the electrical conductance is proportional to

the second power. As the exponent increases, flow is increasingly concentrated in fewer pathways, which become increasingly tortuous. This means that permeability is affected by the pore space structure and its heterogeneity more than formation factor.

4.2.2 Network 2

Results from Network 2 are shown in Figure 4.7. Like Network 1, permeability increases, while formation factor decreases with increasing network size. Compared to Network 1, the value of permeability is nearly two orders of magnitude greater and the value of formation factor is one order of magnitude smaller in Network 2. The permeability plots shown in Figures 4.6 and 4.7 suggest that the REV value for Network 2 is greater than for Network 1. Although the permeability in Network 1 does not vary with scale, for a network size of 6770 μm (Figure 4.6), such as Network 2, permeability tends to keep increasing with scale. This clearly shows that Network 2 is more heterogeneous than Network 1. This pore-scale heterogeneity is because the pore-throat radius distribution in the former is broader than that in the latter (Figure 4.2).

As can be seen in Figure 4.7, the proposed theoretical models estimate the scale-dependent permeability in Networks 2.1 and 2.2 reasonably well. The value of RMSLE ranges from 0.0022 to 0.0103 for the estimations by Eq. (23) and from 0.0014 to 0.0077 for those by Eq. (24). Average RE values for Eqs. (23) and (24) are equal to -1.42 and -0.42%, respectively. These values are less than those reported for Network 1 (see Table 4.1). This may be because Eqs. (23)-(26) were developed based on concepts from CPA, a theory that works best in heterogeneous media with broad pore-throat radius distributions (Hunt, 2001; Hunt et al., 2014). The average RAE values reported for Eqs. (23) and (24) also indicate that Eq. (24) estimates the scale dependence of permeability more accurately than Eq. (23).

Similar to results from Network 1, both Eqs. (25) and (26) overestimate the scale dependence of the formation factor in Network 2. We found that, on average, Eq. (25) estimates $F(L)$ with RE = 2.14% and Eq. (26) with RE = 1.84%. Since both models overestimate F, the values of RE and RAE are the same (Table 4.1). Eq. (26) estimates $F(L)$ more precisely than Eq. (25) because the value of the exponent β in Eq. (26) was optimized from the simulations at the smallest network size (i.e., 1130 μm).

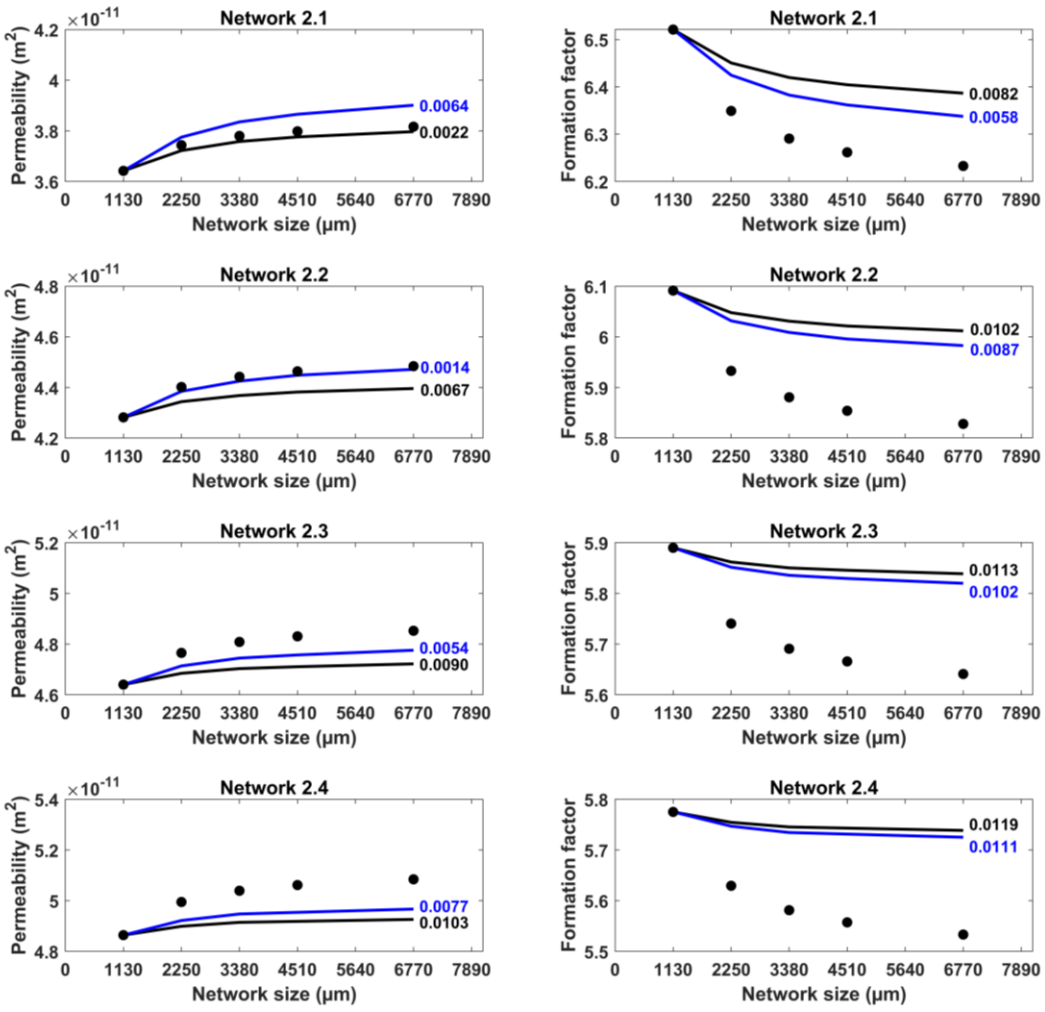

Figure 4.7. Simulated and estimated permeability and formation factor for Network 2. Black filled circles indicate simulation values. Black and blue lines represent estimations by Eqs. (23) and (24) for the permeability and by Eqs. (25) and (26) for the formation factor, respectively. The calculated RMSLE value for each model is given adjacent to each line using the same color code.

4.2.3 Network 3

The pore-throat radius distributions in Network 3 are broader than those in Networks 1 and 2 and, thus, it is the most heterogeneous network among these three cases. The increase in permeability with increasing network sizes (e.g., 6770 μm) indicates that the REV has not been reached (Figure 4.8), which is similar to the results from Network 2 (Figure 4.7). As reported in Figure 4.8, we found 0.0022 < RMSLE < 0.0065 for Eq. (23) and 0.0013 < RMSLE < 0.014 for Eq. (24) in the estimation of the scale dependence of permeability in Network 3. Eq. (24) estimated $k(L)$ more accurately than Eq. (23) (i.e., smaller relative errors) in Networks 3.3 and 3.4 (Table 4.1). However, the source of error in Networks 3.1 and 3.2 is not clear yet.

Based on the average RE values reported in Table 4.1, overall Eq. (23) estimates the scale dependence of permeability in Network 3 more accurately than Eq. (24). More specifically, we found RE = -0.53 and 0.7% and RAE = 0.9 and 1.15%, respectively, for Eqs. (23) and (24). Although Eq. (24) estimates the scale dependence of permeability more accurately than Eq. (23) in Networks 1 and 2, Eq. (23) has higher accuracy than Eq. (24) in Network 3. The reason is yet not clear and requires further investigation.

Results of the formation factor and its scale-dependent estimations are also presented in Figure 4.8. Similar to Networks 1 and 2, Eq. (26) provides more accurate estimations of $F(L)$ than Eq. (25) (see the RMSLE values reported in Figure 4.8). The average RE and RAE values reported in Table 4.1 confirm the obtained results.

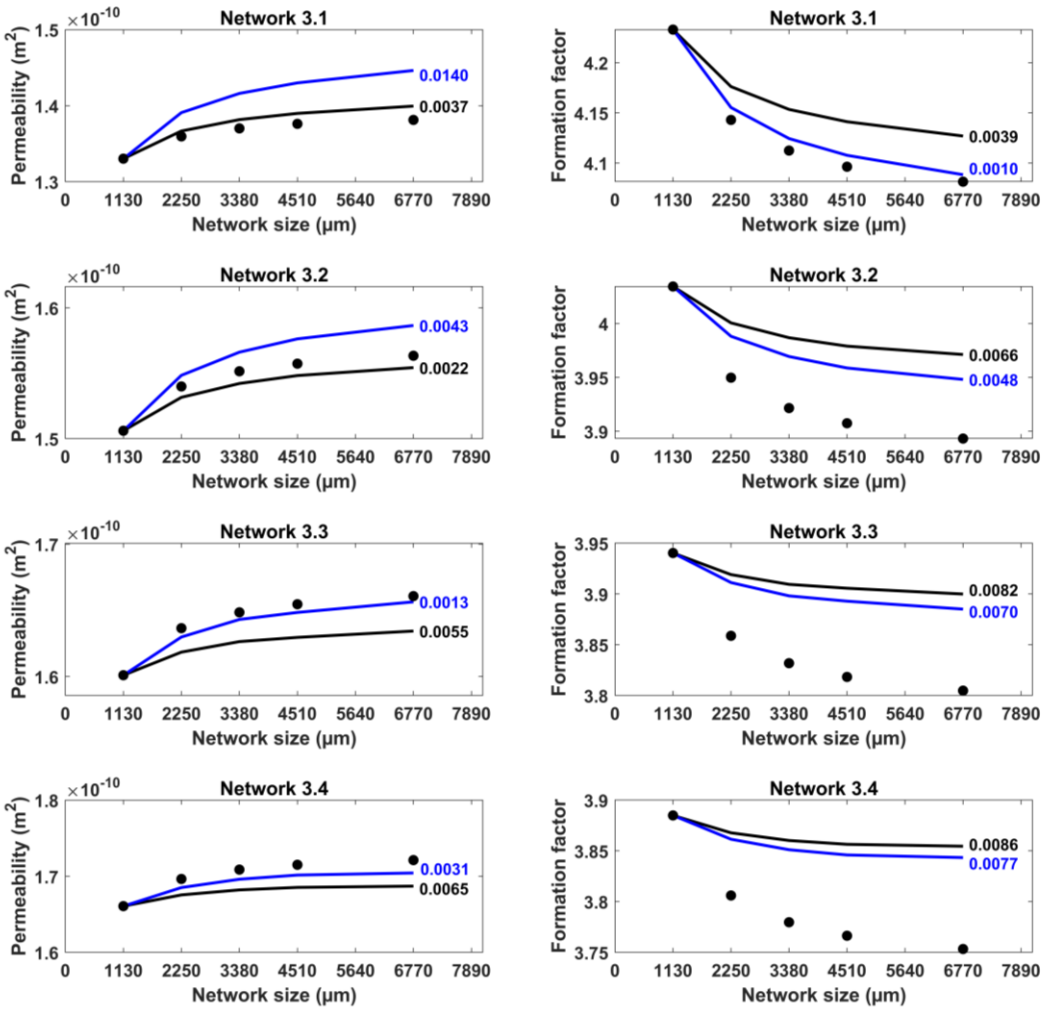

Figure 4.8. Simulated and estimated permeability and formation factor for Network 3. Black filled circles indicate simulation values. Black and blue lines represent estimations by Eqs. (23) and (24) for the permeability and by Eqs. (25) and (26) for the formation factor, respectively. The calculated RMSLE value for each model is given adjacent to each line using the same color code.

4.3. Estimating the scale dependency of permeability from formation factor and/or pore-throat radius distribution

In this section, we present the results of $k(L)$ estimated by Eq. (27) from $k(L_{min})$ and $F(L)$ as well as by Eq. (28) from the pore-throat radius distribution and the simulated formation factor. Figure 4.9 shows the results of $k(L)$ estimations via Eqs. (27) and (28). The RMSLE values for

Network 1 range from 0.0020 to 0.0024 and from 0.0106 to 0.0163 for Eqs. (27) and (28), respectively. As can be seen in Table 4.2, for Eq. (27) and Network 1 we found the average RE = -0.38%, which is considerably less than values reported for Eqs. (23) and (24) in Table 4.1. For Eq. (28) and Network 1 the average RE value is 2.84%, greater than that for Eq. (27). The source of uncertainty in the estimations by Eq. (28) may be due to error in the estimation of $k(L_{min})$. Recall that Eqs. (23), (24), and (27) estimate $k(L)$ from $k(L_{\min})$ as well as the pore-throat radius distribution and/or formation factor, while in Eq. (28) $k(L_{\min})$ is estimated from the pore-throat radius distribution and $F(L_{\min})$.

Results of the scale-dependent permeability estimations using Eqs. (27) and (28) for Network 2 are also shown in Figure 4.9. We found 0.0005 < RMSLE < 0.0007 for Eq. (27) and 0.0013< RMSLE < 0.0117 for Eq. (28). Similar to the results from Network 1, Eq. (27) provides more accurate estimations of $k(L)$ than Eq. (28). This is confirmed through the average RE and RAE values reported in Table 4.2. Comparing the RE values obtained from Eqs. (27) and (28) indicates that the error in the $k(L)$ estimation decreases from Network 1 to Network 2. As stated earlier, Network 2 is more heterogeneous, and its pore-throat radius distribution is broader compared to Network 1 (see Figure 4.2). Since both Eqs. (27) and (28) are based on the CPA, one should expect the improvement of $k(L)$ estimations as the pore-throat radius distribution becomes broader.

The scale-dependent permeability estimations using Eq. (27) and Eq. (28) for Network 3 show results similar to Networks 1 and 2. The RMSLE values for Network 3 ranges between 0.0003 and 0.0006 for Eq. (27) and between 0.0008 and 0.006 for Eq. (28). In Network 3, Eq. (28) underestimates $k(L)$ in all pore-networks except Network 3.1 (see negative RE values in

Table 4.2). We found that the average RAE= 0.09 and 0.91% (Table 4.2), which clearly demonstrates that Eq. (27) provides more accurate estimations than Eq. (28).

Table 4.2. Calculated values of relative error (RE) and relative absolute error (RAE) for theoretical models developed to estimate the scale dependence of permeability in twelve pore networks using Eq. (27) and Eq. (28).

Pore network	Permeability *k*			
	Eq. (27)		Eq. (28)	
	RE	RAE	RE	RAE
1.1	-0.42	0.42	3.80	3.80
1.2	-0.42	0.42	2.45	2.45
1.3	-0.33	0.33	2.57	2.57
1.4	-0.34	0.34	2.53	2.53
Average	-0.38	0.38	2.84	2.84
2.1	-0.10	0.10	2.72	2.72
2.2	-0.13	0.13	1.27	1.27
2.3	-0.10	0.10	0.93	0.93
2.4	-0.10	0.10	0.30	0.30
Average	-0.11	0.11	1.31	1.31
3.1	-0.07	0.07	1.38	1.38
3.2	-0.11	0.11	-0.14	0.17
3.3	-0.11	0.11	-0.68	1.06
3.4	-0.08	0.08	-0.65	1.03
Average	-0.09	0.09	-0.02	0.91
Overall Average	-0.19	0.19	1.20	1.69

*values are in percentage

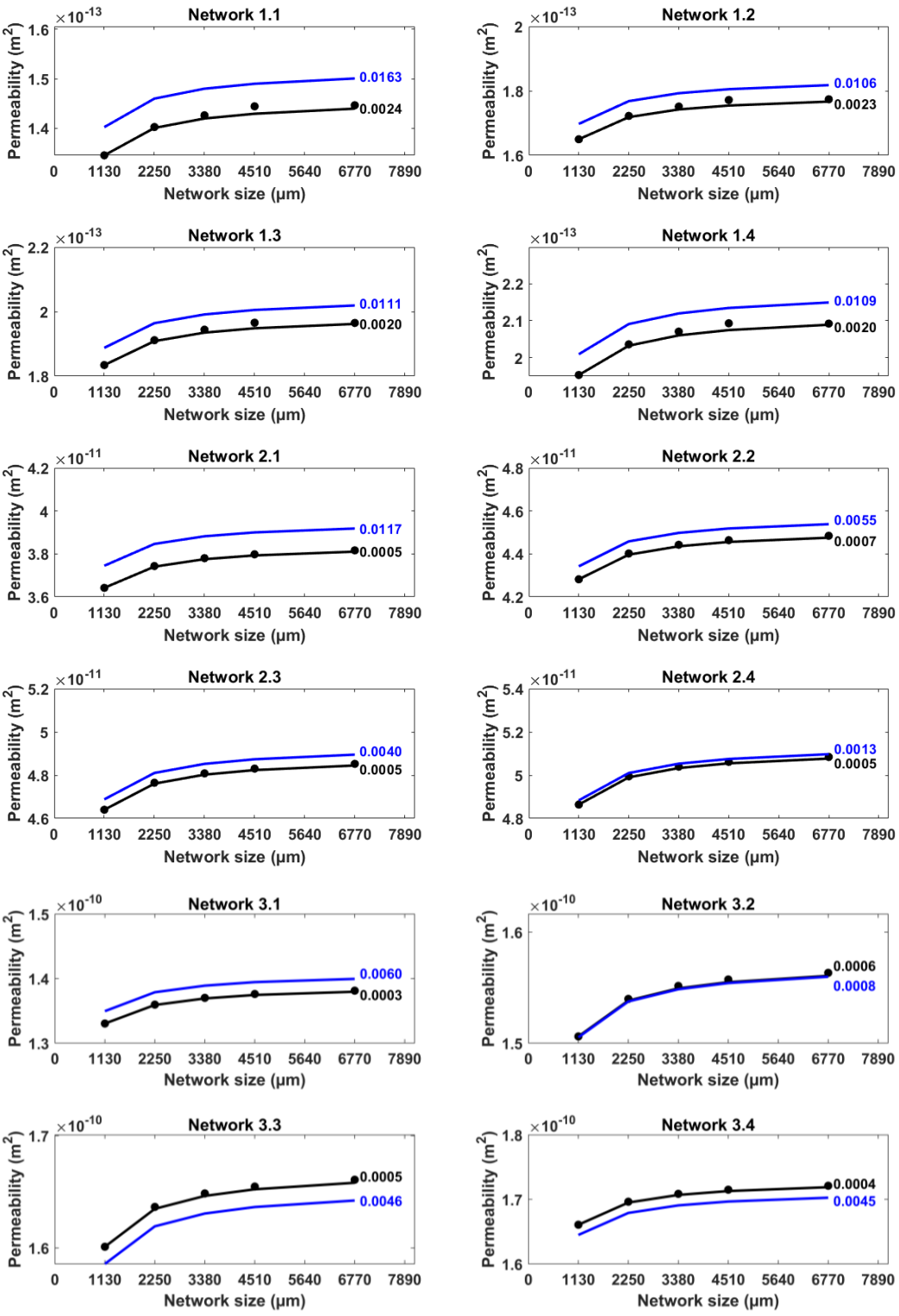

Figure 4.9. Simulated and estimated permeability for the twelve pore-networks. Black filled circles indicate simulation values. Black and blue lines represent estimations by Eqs. (27) and (28), respectively. The calculated RMSLE value for each model is given adjacent to each line using the same color code.

Chapter 5 - Discussion

5.1. Model Accuracy

The RE and RAE values as well as their averages over all the networks for Eqs. (23)-(28) are reported in Tables 4.1 and 4.2. As can be seen, the RE value was found to be less than 5%, which indicates all the proposed models estimated the scale dependence of permeability and formation factor with high accuracy. Comparing the overall average RE and RAE values reported in Tables 4.1 and 4.2 demonstrates that Eq. (27) estimates $k(L)$ more accurately than other models developed in this study. More specifically, in the estimation of $k(L)$ we found the average RE = -1.6, -0.46, -0.19, and 1.2% for Eqs. (23), (24), (27), and (28), respectively. In fact, although Eq. (27) provides a simple relationship, it yields the most accurate estimations among all the models for the networks studied here. This may be because the pore-throat radius distribution does not statistically vary from one scale to another, and the small-scale heterogeneity was appropriately captured by the formation factor across scales. Thus, Eq. (27) which only incorporates $F(Lmin), F(L)$, and $k(Lmin)$ and not r_{tc} has smaller RE values. After Eq. (27), Eq. (24) provides the most accurate estimations of $k(L)$.

For the formation factor, our results show that Eq. (26) with the average RE = 2.04% estimates $F(L)$ slightly better than Eq. (25) with the average RE = 2.38%. In the estimation of the scale dependence of the formation factor, the average RE and RAE values decrease from Network 1 to 3 (Table 4.1). In the estimation of $k(L)$, the same trend was observed for Networks 1 and 2. However, from Network 2 to 3, the average RE and RAE increases for Eq. (24). Further investigations are required to evaluate the proposed models using a broader range of pore networks with broader levels of heterogeneity.

5.2. Limitations

The proposed theoretical scale-dependent models for the permeability and formation factor were developed based on several fundamental assumptions, one of which is that the pore-throat radius distribution does not greatly vary from one scale (or sample volume) to another. This assumption may be valid in pore-network simulations in which pore-throat radius distributions from different scales are statistically the same. However, it is not necessarily observed in natural porous media, such as rocks that are heterogeneous in terms of pore space across scales (Chen, et al., 2015; Han et al., 2016; Tinni et al., 2012).

Our proposed models are limited to experiments and/or simulations that show increasing permeability and decreasing formation factors with scale increase. That is because, based on Eq. (21), as the system size L increases, the critical pore-throat radius r_{tc} increases and approaches r_{tmax} for $L \to \infty$. Since permeability is directly proportional and formation factor is inversely proportional to r_{tc}, k is expected to increase and F is expected to decrease as the system length increases, according to Eqs. (23) to (26). Although increasing $k(L)$ has been widely observed in experiments (Cui et al., 2009; Pachepsky et al., 2014; Schulze-Makuch et al., 1999; Tinni et al., 2012) (see Figure 5.1) and numerical simulations on 3D images (Aslannejad et al., 2017; Jing et al., 2016; Wu et al., 2019; Yu et al., 2020), there exist evidence in the literature (Bernabé et al., 2003; Sahimi et al., 1986; Tahmasebi et al., 2016) that k may decrease as scale increases in certain cases.

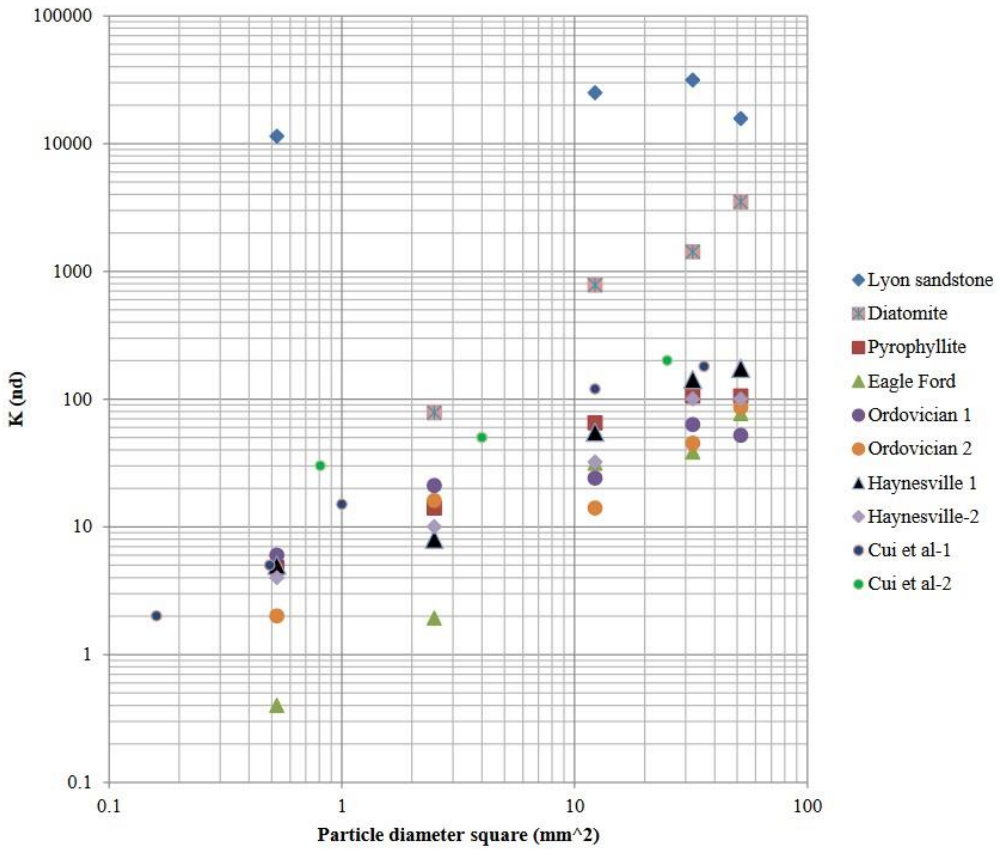

Figure 5.1. Permeability versus particle size squared for experimental data of different rocks (after Tinni et al., 2012). Data from Cui et al. (2009) are also included.

In fact, the value of permeability depends on pore space characteristics, such as porosity, pore connectivity (coordination number), surface area, etc. If such properties vary across scales, depending on their trend and overall interactions, permeability may increase or decrease with increase in system size. Cui et al. (2009) studied the scale dependency of permeability in shales of particles of sizes from nearly 0.2 to 20 mm (see their Fig. 10). They stated that shales crushed into particles of millimeter scale showed strong dual-pore structures. Cui et al. (2009) argued that permeability in smaller particles most probably represents intact matrix properties in fractured reservoir rocks. However, at larger field scales, fractures on scales from micrometers to meters may contribute to flow, and fractures and their networks have different transport properties than

pores in the intact matrix. In another study, Tinni et al. (2012) measured GRI (Gas Research Institute) permeability on crushed shale samples with particle sizes ranged from 0.7 to 6 mm. They reported permeability increase with particle size increase. Tinni et al. (2012) argued that such an increase in GRI permeability was due to change in pore structure from one particle size to another and supported their statement using mercury porosimetry measurements.

Chapter 6 - Conclusion

Modeling the scale dependency of transport modes in porous media has been challenging for various research areas e.g., hydrology, geosciences and petroleum engineering. The scale dependence of flow and transport is attributed to small- and large-scale heterogeneities, such as pores and their size distribution, pore connectivity, long-range correlations, fractures and faults orientations, and spatial and temporal variations. In this study, we investigated the effect of scale on permeability and formation factor via pore-scale numerical simulations. Based on percolation theory and by extending the Hunt (2006) approach, scale-dependent models were developed for permeability and formation factor. Generally, permeability is measured on small samples in the laboratory setting, whereas for practical applications, we need to perform large-scale measurements (field scale) of permeability that often have time consuming and costly methodology. The models proposed in this study offer a way for estimating permeability at large scale by taking into account the permeability at a smaller scale as well as the properties of the porous media such as its pore-throat size distribution and/or formation factor. Comparing with pore-network simulations showed that all the proposed theoretical models estimated k and F accurately with relative errors less than 5%. Further investigations are required to evaluate the proposed models using a broader range of pore networks with broader levels of heterogeneity as well as experimental measurements.

References

Adler, P.M., Jacquin, C.G., Thovert, J.F., 1992. The formation factor of reconstructed porous media. Water Resour. Res. https://doi.org/10.1029/92WR00059

Aslannejad, H., Hassanizadeh, S.M., Raoof, A., de Winter, D.A.M., Tomozeiu, N., van Genuchten, M.T., 2017. Characterizing the hydraulic properties of paper coating layer using FIB-SEM tomography and 3D pore-scale modeling. Chem. Eng. Sci. 160, 275–280. https://doi.org/10.1016/j.ces.2016.11.021

Assouline, S., Selker, J., 2017. Introduction and evaluation of a Weibull hydraulic conductivity-pressure head relationship for unsaturated soils. Water Resour. Res. 53, 4956–4964.

Baychev, T.G., 2018. Pore Space Structure Effects on Flow in Porous Media. PQDT - Glob. The University of Manchester.

Bear, J., 1972. Dynamics of Fluids in Porous Media. Elsevier, New York.

Berg, C.F., 2014. Permeability Description by Characteristic Length, Tortuosity, Constriction and Porosity. Transp. Porous Media 103, 381–400. https://doi.org/10.1007/s11242-014-0307-6

Bernabé, Y., Bruderer-Weng, C., Maineult, A., 2003. Permeability fluctuations in heterogeneous networks with different dimensionality and topology. J. Geophys. Res. Solid Earth 108. https://doi.org/10.1029/2002JB002326

Brace, W.F., 1984. Permeability of crystalline rocks: New in situ measurements. J. Geophys. Res. Solid Earth 89, 4327–4330.

Cao, G., Lin, M., Ji, L., Jiang, W., Yang, M., 2019. Characterization of pore structures and gas transport characteristics of Longmaxi shale. Fuel 258, 116146. https://doi.org/10.1016/j.fuel.2019.116146

Cao, Z., Liu, G., Zhan, H., Li, C., You, Y., Yang, C., Jiang, H., 2016. Pore structure characterization of Chang-7 tight sandstone using MICP combined with N2GA techniques and its geological control factors. Sci. Rep. 6, 36919.

Chen, Y., Wei, L., Mastalerz, M., and Schimmelmann, A., 2015. The effect of analytical particle size on gas adsorption porosimetry of shale. Int. J. Coal Geol. 138, 103–112.

Cui, J., Cheng, L., 2017. A theoretical study of the occurrence state of shale oil based on the pore sizes of mixed Gaussian distribution. Fuel 206, 564–571. https://doi.org/10.1016/j.fuel.2017.06.047

Cui, X., Bustin, A.M.M., Bustin, R.M., 2009. Measurements of gas permeability and diffusivity of tight reservoir rocks: Different approaches and their applications. Geofluids 9, 208–223. https://doi.org/10.1111/j.1468-8123.2009.00244.x

Daigle, H., 2016. Application of critical path analysis for permeability prediction in natural porous media. Adv. Water Resour. 96, 43–54. https://doi.org/10.1016/j.advwatres.2016.06.016

Davudov, D., Moghanloo, R.G., 2017. Scale-Dependent Pore and Hydraulic Connectivity of Shale Matrix. Energy & Fuels acs.energyfuels.7b02619. https://doi.org/10.1021/acs.energyfuels.7b02619

De La Garza Martínez, P.A., 2016. Pore Network Modeling: Alternative Methods to Account for Trapping and Spatial Correlation 72.

Ewing, R.P., Hu, Q., Liu, C., 2010. Scale dependence of intragranular porosity, tortuosity, and diffusivity. Water Resour. Res. 46, 1–12. https://doi.org/10.1029/2009WR008183

Ewing, R.P., Hunt, A.G., 2006. Dependence of the Electrical Conductivity on Saturation in Real Porous Media. Vadose Zo. J. 5, 731. https://doi.org/10.2136/vzj2005.0107

Fallico, C., De Bartolo, S., Troisi, S., Veltri, M., 2010. Scaling analysis of hydraulic conductivity and porosity on a sandy medium of an unconfined aquifer reproduced in the laboratory. Geoderma 160, 3–12. https://doi.org/10.1016/j.geoderma.2010.09.014

Feng, S., Halperin, B.I., Sen, P.N., 1987. Transport properties of continuum systems near the percolation threshold. Phys. Rev. B 35, 197–214. https://doi.org/10.1103/PhysRevB.35.197

Friedman, S.P., Seaton, N.A., 1998. Critical path analysis of the relationship between permeability and electrical conductivity of three-dimensional pore networks. Water Resour. Res. 34, 1703–1710. https://doi.org/10.1029/98WR00939

Garbesi, K., Sextro, R.G., Robinson, A.L., Wooley, J.D., Owens, J.A., Nazaroff, W.W., 1996. Scale dependence of soil permeability to air: Measurement method and field investigation. Water Resour. Res. 32, 547–560. https://doi.org/10.1029/95WR03637

Ghanbarian, B., 2020. Applications of critical path analysis to uniform grain packings with narrow conductance distributions: I. Single-phase permeability. Adv. Water Resour. 137, 103529. https://doi.org/10.1016/j.advwatres.2020.103529

Ghanbarian, B., Hunt, A.G., Sahimi, M., Ewing, R.P., Skinner, T.E., 2013. Percolation Theory Generates a Physically Based Description of Tortuosity in Saturated and Unsaturated Porous Media. Soil Sci. Soc. Am. J. 77, 1920. https://doi.org/10.2136/sssaj2013.01.0089

Ghanbarian, B., Hunt, A.G., Skaggs, T.H., Jarvis, N., 2017. Upscaling soil saturated hydraulic conductivity from pore throat characteristics. Adv. Water Resour. 104, 105–113. https://doi.org/10.1016/j.advwatres.2017.03.016

Ghanbarian, B., Liang, F., Liu, H.H., 2020. Modeling gas relative permeability in shales and tight porous rocks. Fuel 272, 117686.

Ghanbarian, B., Male, F., 2021. Theoretical power-law relationship between permeability and

formation factor. J. Pet. Sci. Eng. 198, 108249. https://doi.org/10.1016/j.petrol.2020.108249

Ghanbarian, B., Taslimitehrani, V., Dong, G., Pachepsky, Y.A., 2015. Sample dimensions effect on prediction of soil water retention curve and saturated hydraulic conductivity. J. Hydrol. 528, 127–137. https://doi.org/10.1016/j.jhydrol.2015.06.024

Ghanbarian, B., Torres-Verdín, C., Skaggs, T.H., 2016. Quantifying tight-gas sandstone permeability via critical path analysis. Adv. Water Resour. 92, 316–322. https://doi.org/10.1016/j.advwatres.2016.04.015

Halperin, B.I., Feng, S., Sen, P.N., 1985. Differences between lattice and continuum percolation transport exponents. Phys. Rev. Lett. 54, 2391–2394. https://doi.org/10.1103/PhysRevLett.54.2391

Han, H., Cao, Y., Chen, S.J., Lu, J.G., Huang, C.X., Zhu, H.H., Zhan, P. and Gao, Y., 2016. Influence of particle size on gas-adsorption experiments of shales: An example from a Longmaxi Shale sample from the Sichuan Basin, China. Fuel 186, 750–757.

Hidajat, I., Mohanty, K.K., Flaum, M., Hirasaki, G., 2002. Study of vuggy carbonates using X-ray CT scanner and NMR, in: SPE Annual Technical Conference and Exhibition, 29 September-2 October. iety of Petroleum Engineers, San Antonio, Texas, p. SPE-77396-MS.

Hopmans, J.W., Nielsen, D.R., Bristow, K.L., 2002. How useful are small-scale soil hydraulic property measurements for large-scale vadose zone modeling? Geophys. Monogr. Ser. 129, 247–258. https://doi.org/10.1029/129GM20

Hsieh, P.A., Neuman, S.P., Stiles, G.K., Simpson, E.S., 1985. Field Determination of the Three-Dimensional Hydraulic Conductivity Tensor of Anisotropic Media: 2. Methodology and Application to Fractured Rocks. Water Resour. Res. 21, 1667–1676. https://doi.org/10.1029/WR021i011p01667

Hunt, A.G., 2006. Scale-dependent hydraulic conductivity in anisotropic media from dimensional cross-over. Hydrogeol. J. 14, 499–507. https://doi.org/10.1007/s10040-005-0453-6

Hunt, A.G., 2003. Some comments on the scale dependence of the hydraulic conductivity in the presence of nested heterogeneity. Adv. Water Resour. https://doi.org/10.1016/S0309-1708(02)00096-9

Hunt, A.G., 2001. Applications of percolation theory to porous media with distributed local conductances. Adv. Water Resour. 24, 279–307. https://doi.org/10.1016/S0309-1708(00)00058-0

Hunt, A.G., 1998. Upscaling in Subsurface Transport Using Cluster Statistics of Percolation. Transp. Porous Media 30, 177–198. https://doi.org/10.1023/A:1006534922791

Hunt, A.G., Ewing, R., Ghanbarian, B., 2014. Percolation theory for flow in porous media.

Hyun, Y., Neuman, S.P., Vesselinov, V. V., Illman, W.A., Tartakovsky, D.M., Di Federico, V., 2002. Theoretical interpretation of a pronounced permeability scale effect in unsaturated fractured tuff. Water Resour. Res. 38, 28-1-28–8. https://doi.org/10.1029/2001wr000658

Ingham, D.B., Pop, I., 2005. Transport Phenomena in Porous Media III, Transport Phenomena in Porous Media III. Elsevier. https://doi.org/10.1016/B978-0-08-044490-1.X5003-0

Iversen, B. V, Moldrup, P., Schjonning, P., Loll, P., 2001. Air and water permeability in differently textured soils at two measurement scales. Soil Sci. 166, 643-659. https://doi.org/Doi 10.1097/00010694-200110000-00001

Jing, Y., Armstrong, R.T., Ramandi, H.L., Mostaghimi, P., 2016. Coal cleat reconstruction using micro-computed tomography imaging. Fuel 181, 286–299. https://doi.org/10.1016/j.fuel.2016.04.127

Joekar-Niasar, V., van Dijke, M.I.J., Hassanizadeh, S.M., 2012. Pore-Scale Modeling of Multiphase Flow and Transport: Achievements and Perspectives. Transp. Porous Media. https://doi.org/10.1007/s11242-012-0047-4

Katz, A.J., Thompson, A.H., 1987. Prediction of rock electrical conductivity from mercury injection measurements. J. Geophys. Res. 92, 599–607. https://doi.org/10.1029/JB092iB01p00599

Katz, A.J., Thompson, A.H., 1986. Quantitative prediction of permeability in porous rock. Phys. Rev. B 34, 8179–8181.

Kogut, P.M., Straley, J.P., 1979. Distribution-induced non-universality of the percolation conductivity exponents. J. Phys. C Solid State Phys. 12, 2151–2159. https://doi.org/10.1088/0022-3719/12/11/023

Mahmoodlu, M.G., Raoof, A., Bultreys, T., Van Stappen, J., Cnudde, V., 2020. Large-scale pore network and continuum simulations of solute longitudinal dispersivity of a saturated sand column. Adv. Water Resour. https://doi.org/10.1016/j.advwatres.2020.103713

McPhee, C., Reed, J., Zubizarreta, I., 2015. Capillary Pressure, in: Developments in Petroleum Science. https://doi.org/10.1016/B978-0-444-63533-4.00009-3

Miller, E.E., Miller, R.D., 1956. Physical theory for capillary flow phenomena. J. Appl. Phys. 27, 324–332. https://doi.org/10.1063/1.1722370

Moradllo, M.K., Qiao, C., Isgor, B., Reese, S., Weiss, W.J., 2018. Relating formation factor of concrete to water absorption. ACI Mater. J. https://doi.org/10.14359/51706844

Naraghi, M.E., Javadpour, F., 2015. A stochastic permeability model for the shale-gas systems. Int. J. Coal Geol. 140, 111–124. https://doi.org/10.1016/j.coal.2015.02.004

Nelson, P.H., 1994. Permeability-porosity relationships in sedimentary rocks. Log Anal. 583.

Nemes, A., Schaap, M.G., Leij, F.J., Wösten, J.H.M., 2001. Description of the unsaturated soil hydraulic database UNSODA version 2.0. J. Hydrol. https://doi.org/10.1016/S0022-1694(01)00465-6

Neuman, S.P., Walter, G.R., Bentley, H.W., Ward, J. J., Gonzalez, D.D., 1984. Determination of horizontal aquifer anisotropy with three wells. GroundWater 22, 66–72.

Niemann, W.L., Rovey II, C.W., 2009. A systematic field-based testing program of hydraulic conductivity and dispersivity over a range in scale. Hydrogeol. J. 17, 307–320.

Pachepsky, Y.A., Guber, A.K., Yakirevich, A.M., McKee, L., Cady, R.E., Nicholson, T.J., 2014. Scaling and Pedotransfer in Numerical Simulations of Flow and Transport in Soils. Vadose Zo. J. 13, 0. https://doi.org/10.2136/vzj2014.02.0020

Rahimpour-Bonab, H., Aliakbardoust, E., 2014. Pore facies analysis: Incorporation of rock properties into pore geometry based classes in a Permo-Triassic carbonate reservoir in the Persian Gulf. J. Geophys. Eng. https://doi.org/10.1088/1742-2132/11/3/035008

Raoof, A., 2011. Reactive/Adsorptive Transport in (Partially-) Satu- rated Porous Media; from pore scale to core scale. Utrecht University.

Revil, A., Binley, A., Mejus, L., Kessouri, P., 2015. Predicting permeability from the characteristic relaxation time and intrinsic formation factor of complex conductivity spectra. Water Resour. Res. https://doi.org/10.1002/2015WR017074

Rovey, C.W., Cherkauer, D.S., 1995. Scale Dependency of Hydraulic Conductivity Measurements. Groundwater 33, 769–780. https://doi.org/10.1111/j.1745-6584.1995.tb00023.x

Sadeghi, M., Ghahraman, B., Warrick, A.W., Tuller, M., Jones, S.B., 2016. A critical evaluation of the Miller and Miller similar media theory for application to natural soils. Water Resour. Res. 52, 3829–3846.

Sahimi, M., 1994. Applications of Percolation Theory. Taylor and Francis, London.

Sahimi, M., Hughes, B.D., Scriven, L.E., Ted Davis, H., 1986. Dispersion in flow through porous media-I. One-phase flow. Chem. Eng. Sci. 41, 2103–2122. https://doi.org/10.1016/0009-2509(86)87128-7

Saidian, M., Prasad, M., 2015. Effect of mineralogy on nuclear magnetic resonance surface relaxivity: A case study of Middle Bakken and Three Forks formations. Fuel 161, 197–206.

Schulze-Makuch, D., 1996. Facies dependent scale behavior of hydraulic conductivity and longitudinal dispersivity in the carbonate aquifer of Southeastern Wisconsin. University of Wisconsin, Milwaukee.

Schulze-Makuch, D., Carlson, D.A., Cherkauer, D.S., Malik, P., 1999. Scale dependency of hydraulic conductivity in heterogeneous media. Ground Water 37, 904–919.

Sen, P.N., Goode, P.A., Sibbit, A., 1988. Electrical conduction in clay bearing sandstones at low and high salinities. J. Appl. Phys. https://doi.org/10.1063/1.340476

Sen, P.N., Straley, C., Kenyon, W.E., Whittingham, M.S., 1990. Surface-to-volume ratio, charge density, nuclear magnetic relaxation, and permeability in clay-bearing sandstones. Geophysics. https://doi.org/10.1190/1.1442772

Stauffer, D., Aharony, A., 1994. Introduction to Percolation Theory. Taylor and Francis, London.

Tahmasebi, P., Javadpour, F., Sahimi, M., Piri, M., 2016. Multiscale study for stochastic characterization of shale samples. Adv. Water Resour. 89, 91–103. https://doi.org/10.1016/j.advwatres.2016.01.008

Tinni, A., Fathi, E., Agarwal, R., Sondergeld, C.H., Akkutlu, I.Y., Rai, C.S., 2012. Shale permeability measurements on plugs and crushed samples, in: SPE Canadian Unconventional Resources Conference. Society of Petroleum Engineers, p. SPE 162235.

Tyč, S., Halperin, B.I., 1989. Random resistor network with an exponentially wide distribution of bond conductances. Phys. Rev. B 39, 877–880. https://doi.org/10.1103/PhysRevB.39.877

Valvatne, P.H., 2004. Predictive pore-scale modelling of multiphase flow. IMPERIAL COLLEGE LONDON.

Wu, H., Yao, Y., Zhou, Y., Qiu, F., 2019. Analyses of representative elementary volume for coal using X-ray M-CT and FIB-SEM and its application in permeability predication model. Fuel 254, 115563. https://doi.org/10.1016/j.fuel.2019.05.146

Xiong, Q., Baychev, T.G., Jivkov, A.P., 2016. Review of pore network modelling of porous media : Experimental characterisations , network constructions and applications to reactive transport. J. Contam. Hydrol. 192, 101–117. https://doi.org/10.1016/j.jconhyd.2016.07.002

Xu, R., Prodanović, M., 2018. Effect of pore geometry on nitrogen sorption isotherms interpretation: A pore network modeling study. Fuel 225, 243–255. https://doi.org/10.1016/j.fuel.2018.03.143

Yoon, H., Dewers, T.A., 2013. Nanopore structures, statistically representative elementary volumes, and transport properties of chalk. Geophys. Res. Lett. 40, 4294–4298. https://doi.org/10.1002/grl.50803

Yu, X., Xu, L., Regenauer-Lieb, K., Jing, Y., Tian, F.B., 2020. Modeling the effects of gas slippage, cleat network topology and scale dependence of gas transport in coal seam gas reservoirs. Fuel 264, 116715. https://doi.org/10.1016/j.fuel.2019.116715

Zapata, Y., Sakhaee-Pour, A., 2016. Modeling adsorption-desorption hysteresis in shales: Acyclic pore model. Fuel 181, 557–565. https://doi.org/10.1016/j.fuel.2016.05.002

Zhao, B., MacMinn, C.W., Primkulov, B.K., Chen, Y., Valocchi, A.J., Zhao, J., Kang, Q., Bruning, K., McClure, J.E., Miller, C.T., Fakhari, A., Bolster, D., Hiller, T., Brinkmann,

M., Cueto-Felgueroso, L., Cogswell, D.A., Verma, R., Prodanović, M., Maes, J., Geiger, S., Vassvik, M., Hansen, A., Segre, E., Holtzman, R., Yang, Z., Yuan, C., Chareyre, B., Juanes, R., 2019. Comprehensive comparison of pore-scale models for multiphase flow in porous media. Proc. Natl. Acad. Sci. U. S. A. https://doi.org/10.1073/pnas.1901619116

Zhao, J., Qin, F., Derome, D., Carmeliet, J., 2020. Simulation of quasi-static drainage displacement in porous media on pore-scale: Coupling lattice Boltzmann method and pore network model. J. Hydrol. https://doi.org/10.1016/j.jhydrol.2020.125080

Appendix A - **Pore-Network generation and flow simulation script**

This script generates pore networks using Netgen, and afterwards executes Poreflow. Pore network characteristics and flow properties such as r_t, r_b, l_t, k, F, porosity and capillary pressure data are saved in separate $.mat$ files for each of the networks.

```
%%%%%%%%%%%%%%%%%%%%%%%%%%%%%%%%%%%%%%%%%%%%%%%%%%%%%%%%%%%%%%%%%%%%%%%%%%%%%%%
clear
clc
close all

networksizes = [10 20 30 40 60];      % network sizes

 deltas= [0.2] ;             % Weibull distribution parameter
 etas= [ 1.8] ;               % Weibull distribution parameter
 min_rt = 0.1;
 max_rt = 10;

%coordination number:
coordnum_list= [6];

iteration1 = 100 ;      % iteration for networksizes of 10 20 30
iteration2 = 100 ;      % iteration for networksizes of 40 60 65

%% %%%%%%%%%%%%%%%%%%%%%%%%%%%%%%%%%%%%%%%%%%%%%%%%%%%%%%%%%%%%%%%%%%%%%%%%%%%%%%%
starttime = datetime;

for j= 1: length(deltas)        % changing delta & eta values

    k_mat =     zeros(length(networksizes),iteration1);  % pre-allocationg
for output matrices of k, f and phi
    f_mat =     k_mat;
    phi_mat =   k_mat;

    Sw = nan* ones(length(networksizes), 200, iteration1);
    Pc = Sw;
    Sw_imb = Sw;
    Pc_imb = Sw;

    delta = deltas(j)
    eta = etas(j)

        for a= 1:length(coordnum_list)
            coordnum = coordnum_list(a);
            currDate = strrep(datestr(datetime), ':', '_');

        for i= 1: length(networksizes)   % changing network size

        % creating the .dat file for input of netgen:
        name= 'A'
        dlmwrite('netappended.dat',name)

        netsize= networksizes(i)* ones(1,3)
        dlmwrite('netappended.dat',netsize,'-append','delimiter',' ')

        rlalphat =[min_rt max_rt delta eta;
```

```
        100 100 0.05 2.8;
        0 0 0.2 18.0;
        0.001 0.04811 0.8 1.6]
        dlmwrite('netappended.dat',rlalphat,'-append','delimiter',' ')

        proport =[ 0 1; 0 1]
        dlmwrite('netappended.dat',proport,'-append','delimiter',' ')

        connec = [0;coordnum]
        dlmwrite('netappended.dat',connec,'-append','delimiter',' ')

        udeperiodic = 'T'
        dlmwrite('netappended.dat',udeperiodic,'-append','delimiter',' ')
% end of network input file generation

        % defining the number of iterations:
        if networksizes(i) > 30
            iteration = iteration2
        else
            iteration = iteration1
        end


        %%% running netgen & then poreflow:

            k= 1; % k is the iteration index
            while k < iteration + 1
            system('netgen_win32.exe netappended.dat' ); % generate network

 %saving pore-throat radii values in:
table_rp= readtable('A_node2.dat');
 rp= table_rp.Var3;

table_rt= readtable('A_link1.dat');
rt= table_rt.Var4;

table_thLength= readtable('A_link2.dat');
lt= table_thLength.Var6;

                if netsize(1) < 21
                    delay = 5
                elseif netsize(1)> 21 && netsize(1)<31
                    delay = 7
                elseif netsize(1)>31 && netsize(1)<46
                    delay= 11
                else delay = 19
                end

                startflow= 'start poreflow_win32.exe runflow.dat ';
                timeout= sprintf('TIMEOUT /T %i',delay)
                kill= 'taskkill /f /im poreflow_win32.exe';
                exitcmd = 'taskkill /f /im cmd.exe';

                fileID = fopen('batchfile.bat','w');
                fprintf(fileID,'%s \n' ,startflow,timeout,kill,exitcmd);


                system('batchfile.bat &')  %simulate flow
```

```
                pause(delay+1)

                cmdout =fileread('runflow.prt');
                fclose all
                newcmdout= splitlines(cmdout);

                %get permability:
                pattern = "Absolute permeability (m2)";
                TF_k = contains(newcmdout,pattern);
                k_line = newcmdout(find(TF_k==1))
                k_linesplit = split(join(k_line));
                k_mat(i,k)= str2double(cell2mat(k_linesplit(end)));

                % get formation factor:
                pattern = "Formation factor:";
                TF_f = contains(newcmdout,pattern);
                f_line = newcmdout(find(TF_f==1))
                f_linesplit = split(join(f_line));
                f_mat(i,k)= str2double(cell2mat(f_linesplit(end)));

                %get porosity:
                pattern = "Net porosity:";
                TF_phi = contains(newcmdout,pattern);
                phi_line = newcmdout(find(TF_phi==1))
                phi_linesplit = split(join(phi_line));
                phi_mat(i,k)= str2double(cell2mat(phi_linesplit(end)));

                %capillary pressure curve:
                runflow_draincycle_1
                sw= Res_draincycle_1(:,1);
                Sw(i,1:length(sw),k)= sw;

                pc= Res_draincycle_1(:,2);
                Pc(i,1:length(pc),k) = pc;

                runflow_imbcycle_2
                sw_imb= Res_imb_2(:,1);
                Sw_imb(i,1:length(sw_imb),k)= sw_imb;
                pc_imb= Res_imb_2(:,2);
                Pc_imb(i,1:length(pc_imb),k) = pc_imb;


                k= k+1
                end

        end

k_mat_init= k_mat;
f_mat_init= f_mat;
phi_mat_init= phi_mat;

k_mat_init(k_mat_init==0)= nan;
f_mat_init(isnan(k_mat_init))= nan;
phi_mat_init(isnan(k_mat_init))= nan;

kk= nanmean(k_mat_init,2);
ff = nanmean(f_mat_init,2);
pp= nanmean(phi_mat_init,2);
```

```
% clean data file % removing iterations which have f<1:
f_mat(f_mat < 1) = nan;
k_mat(find(isnan(f_mat))) = nan;
phi_mat(find(isnan(f_mat))) = nan;


kkk= nanmean(k_mat,2);
fff= nanmean(f_mat,2);
ppp= nanmean(phi_mat,2);

% reading pore-network info
table= readtable('A_link1.dat');
rt= table.Var4;

table_rp= readtable('A_node2.dat');
 rp= table_rp.Var3;

 table_thLength= readtable('A_link2.dat');
 thLength= table_thLength.Var6;

%%%%%%%%%%%%%%%%%  Plots and errorbars  %%%%%%%%%%%%%%%%%%%%%%%%%%%
out = 'outputfiles'
if isdir(out)==0
    mkdir(out)
end

netInfo = sprintf(' delta%0.1f eta%0.1f
maxrt%d_z%0.2f',delta,eta,max_rt,coordnum);
foldername = [currDate netInfo];
mkdir(out,foldername)

path_save= sprintf('%s/%s/',out,foldername)

% plot of k:
stdkkk = nanstd(k_mat,2)
figure
e = errorbar(networksizes,kkk,stdkkk)

 e.Color  = 'red';
 e.Marker = 'o';

tname= sprintf('k vs net size   delta=%0.1f  eta=%0.1f',delta, eta)
title(tname)

figname= sprintf('%s/K_delta%0.1f__eta%0.2f.fig',path_save, delta,eta)
savefig(figname)

% plot of f:
stdfff = nanstd(f_mat,2);
figure
e2= errorbar(networksizes,fff,stdfff)
e2.Color ='red'
 e2.Marker='o'

tname= sprintf('F vs net size   delta=%0.1f  eta=%0.1f', delta, eta)
title(tname)
figname= sprintf('%s/F_delta%0.1f__eta%0.2f.fig',path_save,delta,eta)
```

```
savefig(figname)

% plot of porosity:
stdppp = nanstd(phi_mat,2);
figure
e3= errorbar(networksizes,ppp,stdppp)
e3.Color ='red'
 e3.Marker='o'
tname= sprintf('Porosity vs net size   delta=%0.1f  eta=%0.1f', delta, eta)
title(tname)
figname= sprintf('%s/p_delta%0.1f__eta%f.fig',path_save,delta,eta)
savefig(figname)

p = mfilename('fullpath')

endtime = datetime;
Durationtime = endtime - starttime
% save variables
fname = sprintf('%s/delta%0.2f__eta%0.1f.mat',path_save,delta,eta)
save (fname)

end

end
```

Appendix B - **Sample Netgen input data**

The input into Netgen is a *.dat* file which contains the statistical characteristics of pore network. This input file then is supplied to the pore network generator executable as an argument. Below is a sample of the Netgen input files used in this study.

```
A     % Base file
60 60 60    % Lattice size
0.1 10 0.2 1.8    % Min throat radius, max throat radius, delta exp, eta exp
100 100 0.05 2.8  % Min throat length, max throat length, delta exp, eta exp
0 0 0.2 18  % Min aspect ratio, max aspect ratio, delta exp, eta exp
0.001 0.04811 0.8 1.6   % Triangles: Min G, max G, delta exp, eta exp
0 1   % Pores: proportion of square and circular pores
0 1    % Throats: proportion of square and circular throats
0      % Proportion of pore volume occupied by clay
6     % Average connection number <= 6
T     % Use periodic boundary conditions
```

Appendix C - **Sample Poreflow input data**

A keyword based input file is used by Poreflow to read the pore networks generated by Netgen and simulate flow through them. The input file used in this study is presented below.

```
NETWORK
% bin filename
F A
#
SAT_TARGET
%finalSat maxPc maxDeltaSw maxDeltaPc calcKr calcI
0.00 1.0E21 0.01 500000.0 F F
1.00 -1.0E21 0.01 500000.0 F F
#
EQUIL_CON_ANG
% model min max delta gamma scheme m2_separation
1 0 0 -1.0 -1.0 rand 25.2
#
RES_FORMAT
matlab
```

Appendix D - **Analysis of the data from Katz and Thompson (1986) and Berg (2014)**

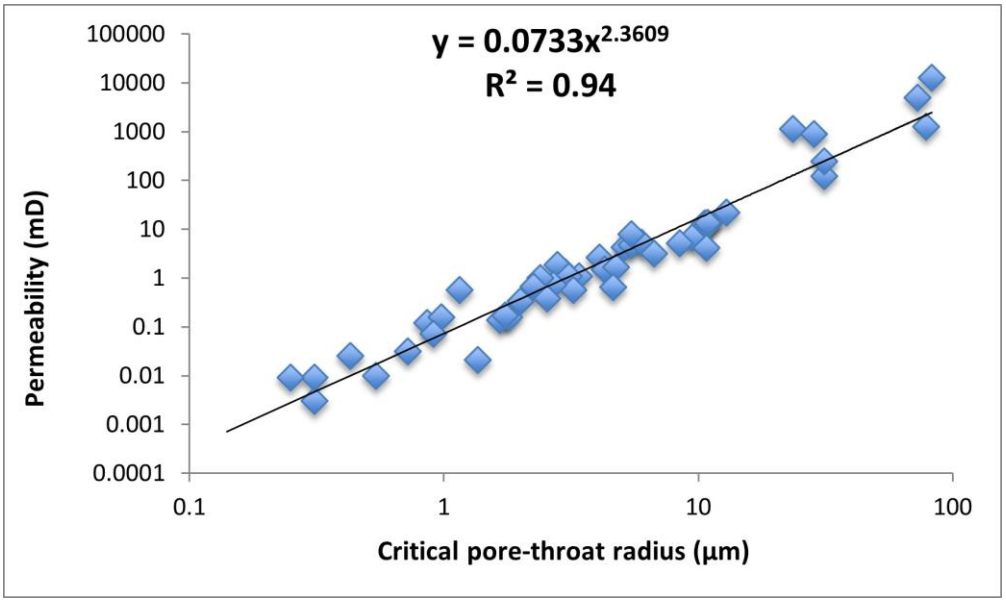

Figure D.1. Plot of permeability against critical pore-throat radius. Data from Katz and Thompson, (1986).

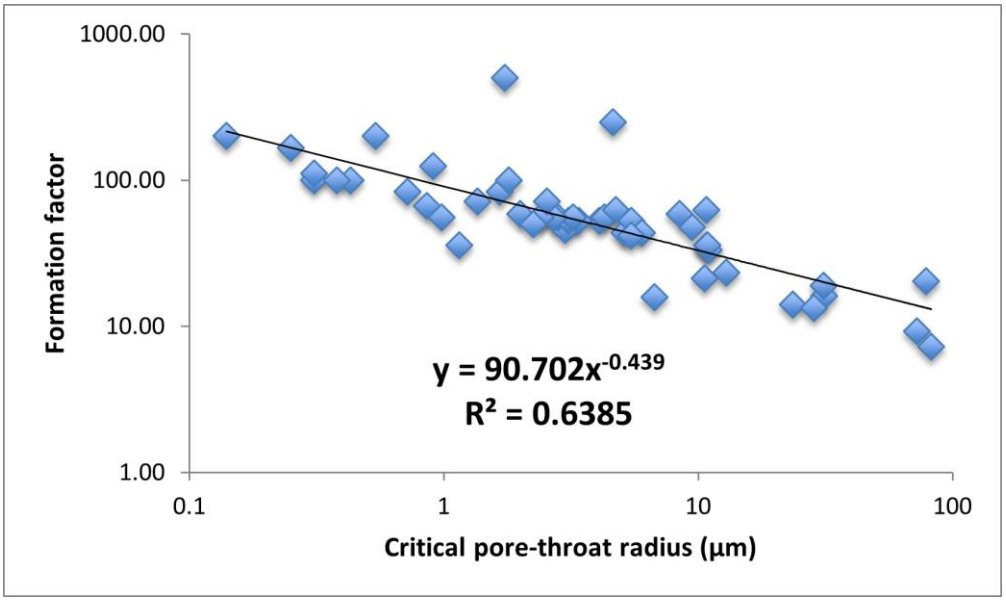

Figure D.2. Plot of formation factor against critical pore-throat radius. Data from Katz and Thompson, (1986).

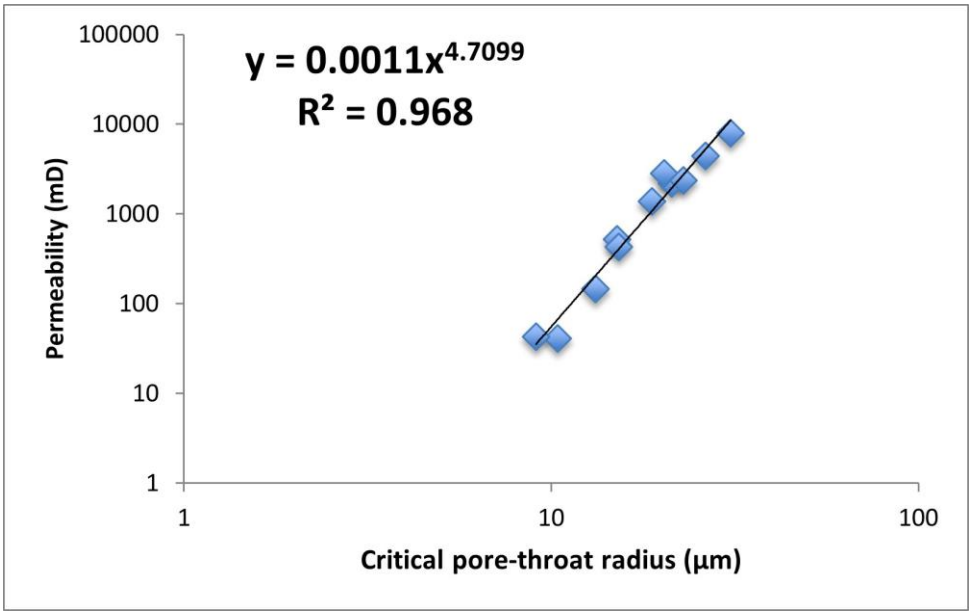

Figure D.3. Plot of permeability against critical pore-throat radius. Data from (Berg, 2014).

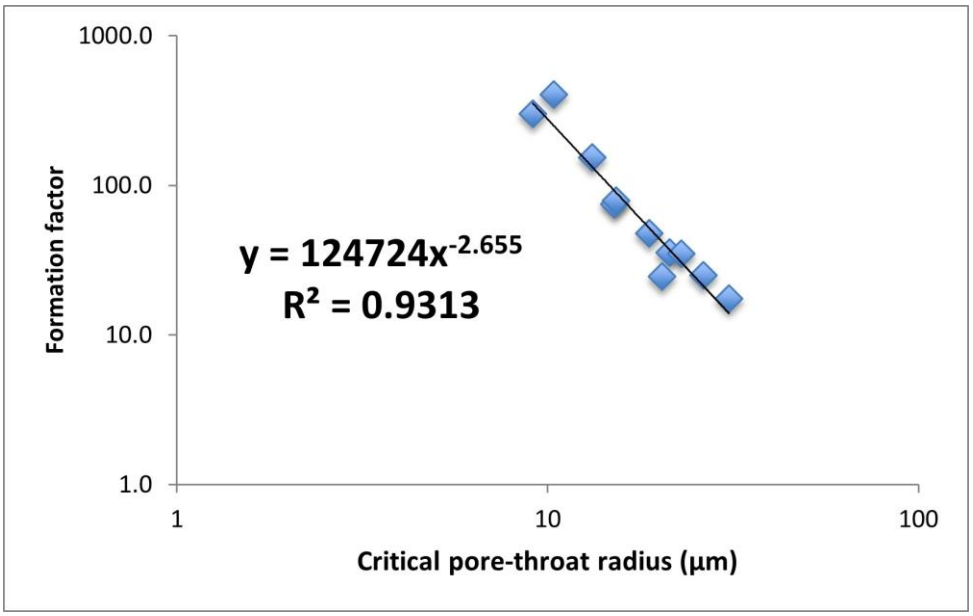

Figure D.4. Plot of formation factor against critical pore-throat radius. Data from (Berg, 2014).

Appendix E - **Scale-Dependent script**

The following script determines the scale dependence of permeability and formation factor using concepts from percolation theory discussed in Chapter 3 (i.e., Eqs. (23)-(28)). Simulated and estimated permeability and formation factor for each of the networks is then plotted in a subplot.

```
%%%%%%%%%%%%%%%%%%%%%%%%%%%%%%%%%%%%%%%%%%%%%%%%%%%%%%%%%%%%%%%%%%%%%%%%%%%%%%%
clc
clear all
close all

etas= [12 18 24 30] ;
deltas= [0.2 0.2 0.2 0.2] ;
maxrt_list = [10 50 75 ];
minrt_list = [0.1 10 1];
subplotmatk = [1 3 5 7];
subplotmatf = [2 4 6 8];
titlelabel10 = [ 1.1 1.1 1.2 1.2 1.3 1.3 1.4 1.4];
titlelabel50 = [ 2.1 2.1 2.2 2.2 2.3 2.3 2.4 2.4];
titlelabel75 = [ 3.1 3.1 3.2 3.2 3.3 3.3 3.4 3.4];

currDate = strrep(datestr(datetime), ':', '_'); % current date and time

% Medium's properties
alpha = 3.3;              % alpha represents exponent in k ~ r_c^(alpha)
beta = 1.37;              % beta represents exponent in F ~ r_c^(-beta)
lt = 100;                 % lt in microns is a fundamental length, or typical
pore throat length
L = [ 10 20 30 40 60];    % L represents the number of sites along each
dimension for a cubic network
La = [1.13006e-003 2.25e-003 3.38e-003 4.51e-003 6.77e-003]*10^6 % La in
microns is the network length

% load data:
perm_data
formatiofactor_data

% rows for etas(12,18,24,30) and columns for rt ranges (10 50 75)
rmsle_k_L_db = zeros(length(etas),length(maxrt_list));
rmsle_k_L_mod_db = rmsle_k_L_db;
k_L_mat = zeros(length(etas),length(L),length(maxrt_list));
k_L_mod_mat = k_L_mat;
f_L_mat = k_L_mat;
f_L_mod_mat = k_L_mat;

for a= 1:length(maxrt_list) % changing rt
    min_rt= minrt_list(a)
    max_rt= maxrt_list(a)
        for b = 1:length(etas) % changing the distribution


k_10 = k_DatabaseSim(b,(1),a);      % Permeability at largest lattice size
```

```
F_10 = f_DatabaseSim(b,(1),a);     % Formation factor at largest lattice size

% creating the .dat file for input of netgen:
        name= 'A'
        dlmwrite('defaultnet.dat',name)

        net = 40
        netsize= net* ones(1,3)
        dlmwrite('defaultnet.dat',netsize,'-append','delimiter',' ')

        delta= deltas(b);
        eta= etas(b);

        rlalphat =[min_rt max_rt delta eta;
        100 100 0.3 2.0;
        0 0 0.2 3.0;
        0.001 0.04811 0.8 1.6]
        dlmwrite('defaultnet.dat',rlalphat,'-append','delimiter',' ')
        proport =[ 0 1; 0 1]
        dlmwrite('defaultnet.dat',proport,'-append','delimiter',' ')

        connec = [0;6]
        dlmwrite('defaultnet.dat',connec,'-append','delimiter',' ')

        udeperiodic = 'T'
        dlmwrite('defaultnet.dat',udeperiodic,'-append','delimiter',' ')


system('netgen_win32.exe defaultnet.dat' ); % generate network
table= readtable('A_link1.dat');
head(table,5);
rt= table.Var4;

[fR, R] = hist(rt.*10^6,40);   % R is pore radius in microns & fR is pore
size distribution
% Normalizing pore size distribution
N = 2000;
r = linspace(min(R),max(R),N);
fr = interp1(R,fR,r,'Makima');

nu = 0.88;                              % Universal scaling exponent for the
correlation length

v = [];
% Determing the total volume of pores (vtot)
for i = 1:1:length(r)
    if i == 1
        v(i) = 0;
    else
        v(i) = r(i).^2 .* fr(i) .* (r(i) - r(i-1));
    end
end
vtot = sum(v);

rc = [];
vc = [];
% Determining the critical pore radius at each network size
```

```
for i = 1:1:length(La)
    for j = 1:1:length(r)
        for k = j:1:length(r)
            if k == j
               vc(k) = 0;
            else
               vc(k) = r(k).^2 .* fr(k) .* (r(k) - r(k-1));
            end
        end
        vt(i,j) = sum(vc);
        fc(i,j) = vt(i,j)./vtot;
        diff(i,j) = abs(fc(i,j) - (lt/(La(i)+lt))^(1/nu));
    end
end

for i = 1:1:length(La)
    ind(i) = find(diff(i,:)==min(diff(i,:)));
    rc(i) = r(ind(i));
end

% Estimating permeability and formation factor at various network sizes
k_L = k_10 .* (rc./rc(1)).^2;
f_L = F_10 .* (rc./rc(1)).^-1;

k_L_mod = k_10 .* (rc./rc(1)).^alpha;
f_L_mod = F_10 .* (rc./rc(1)).^-beta;

%saving  into matrix
k_L_mat(b,:,a)=k_L;
k_L_mod_mat(b,:,a)=k_L_mod;
k_L_new_mat(b,:,a)=k_L_new;
f_L_mat(b,:,a)=f_L;
f_L_mod_mat(b,:,a)=f_L_mod;

%computinng RMSLE:
rmsle_k_L_db(b,a)=RMSLE(k_L,k_DatabaseSim(b,:,a));
rmsle_k_L_mod_db(b,a)=RMSLE(k_L_mod,k_DatabaseSim(b,:,a));
rmsle_f_L_db(b,a)=RMSLE(f_L,f_DatabaseSim(b,:,a));
rmsle_f_L_mod_db(b,a) = RMSLE(f_L_mod,f_DatabaseSim(b,:,a));

out = 'outputPlots'
if isdir(out)==0
    mkdir(out)
end

netInfo = sprintf(' maxrt%d',max_rt);
% foldername = [currDate netInfo];
foldername = [netInfo];

mkdir(out,foldername)

path_save= sprintf('%s/%s/',out,foldername)
%%%permeability subplot:

fontsize =11;
labelfontsize = 12;
axesfontsize = 12
```

```
plotline_width = 2;
markersize = 5;
titlefontsize = 14


if maxrt_list(a) == 10
    titlelabel = titlelabel10;
elseif maxrt_list(a) == 50
    titlelabel = titlelabel50;
else     titlelabel = titlelabel75;
end

k_sub= 10*maxrt_list(a);
figure(k_sub)
subplot(length(etas),2,subplotmatk(b))
set(gcf, 'Units', 'centimeters');
set(gcf, 'Position', [25 1 30 33]);
xlim([0 72])
xticklabels([0 1130 2250 3380 4510 5640 6770 7890]); % network sizes in
micron
hold on
box on

plot(L,k_L,'k','LineWidth',plotline_width)
rmsle_k_L = sprintf('%0.4f ',RMSLE(k_L,k_DatabaseSim(b,:,a)))
text(61,
k_L(end),rmsle_k_L,'FontSize',fontsize,'Color','k','FontWeight','bold','Posit
ion',[61.9177215245753 1.44278983053947e-13 0])

plot(L,k_L_mod,'b','LineWidth',plotline_width)
rmsle_k_L_mod = sprintf('%0.4f ',RMSLE(k_L_mod,k_DatabaseSim(b,:,a)));
text(61,
k_L_mod(end),rmsle_k_L_mod,'FontSize',fontsize,'Color','b','FontWeight','bold
')

plot(networksizes,k_DatabaseSim(b,:,a),'o','LineWidth',plotline_width,'Marker
Size',markersize,...
    'MarkerEdgeColor','k','MarkerFaceColor','k')

set(gca,'fontweight','bold','fontsize',axesfontsize)
xlabel('Network size (μm)','FontWeight','bold', 'FontSize',labelfontsize)
ylabel('Permeability (m^2)','FontWeight','bold', 'FontSize',labelfontsize)
xticks([0 10 20 30 40 50  60 70]);
xticklabels([0 1130 2250 3380 4510 5640 6770 7890]); % network sizes in
micron
title(['Network ',num2str(titlelabel(subplotmatk(b)))])

%%%%%%%%%%%%%%%%%%%%%%%%%%%%%%%%
% formation factor subplot:

subplot(length(etas),2,subplotmatf(b))

xlim([0 72])
xticklabels([0 1130 2250 3380 4510 5640 6770 7890]); % network sizes in
micron

hold on
```

```
box on
plot(L,f_L,'k','LineWidth',plotline_width)
rmsle_f_L = sprintf('%0.4f ',RMSLE(f_L,f_DatabaseSim(b,:,a)));
text(61,f_L(end),rmsle_f_L,'FontSize',fontsize,'Color','k','FontWeight','bold
')
plot(L,f_L_mod,'b','LineWidth',plotline_width)
rmsle_f_L_mod = sprintf('%0.4f ',RMSLE(f_L_mod,f_DatabaseSim(b,:,a)));
text(61,f_L_mod(end),rmsle_f_L_mod,'FontSize',fontsize,'Color','b','FontWeigh
t','bold')

plot(L,f_DatabaseSim(b,:,a),'o','MarkerSize',markersize,'LineWidth',plotline_
width,...
    'MarkerEdgeColor','k','MarkerFaceColor','k')
set(gca,'fontweight','bold','fontsize',axesfontsize)
 xlabel("Network size (µm)"+ newline+"   ",'FontWeight','bold',
'FontSize',labelfontsize)
xticks([0 10 20 30 40 50  60 70]);
 xticklabels([0 1130 2250 3380 4510 5640 6770 7890]); % network sizes in
micron

ylabel('Formation factor','FontWeight','bold', 'FontSize',labelfontsize)
title(['Network ',num2str(titlelabel(subplotmatk(b)))])
        end
end

pause
%note that this code saves the figure in the current folder
figure(100)
savefig('fig100.fig')
print -dtiff -r600 fig100.tiff

figure(500)
savefig('fig500.fig')
print -dtiff -r600 fig500.tiff

figure(750)
savefig('fig750.fig')
print -dtiff -r600 fig750.tiff


%compute mean of rmsle over all networks for each of the models:
mean_rmsle_k_ModelA = mean(rmsle_k_L_db(:))
mean_rmsle_k_ModelB = mean(rmsle_k_L_mod_db(:))

mean_rmsle_f_ModelA = mean(rmsle_f_L_db(:))
mean_rmsle_f_ModelB = mean(rmsle_f_L_mod_db(:))

%compute relative errors:
k_err_ModelA = (k_L_mat- k_DatabaseSim)./k_DatabaseSim;
k_err_ModelA = mean(k_err_ModelA,2)

k_err_ModelB = (k_L_mod_mat- k_DatabaseSim)./k_DatabaseSim;
k_err_ModelB = mean(k_err_ModelB,2)

f_err_ModelA = (f_L_mat- f_DatabaseSim)./f_DatabaseSim;
f_err_ModelA = mean(f_err_ModelA,2)
```

```
f_err_ModelB = (f_L_mod_mat- f_DatabaseSim)./f_DatabaseSim;
f_err_ModelB = mean(f_err_ModelB,2)

% save variables
fname = sprintf('%s/AllVariables.mat',out);
save (fname)


%%%%%%%%%%%%%%%%%%%%%%%%%%%%%%%%%%%%%%%%%%%%%%%%%%%%%%%%%%%%%%%%%%%%%%%%%%%
This following script plots the estimated permeabilities using Eq. (27) and
Eq. (28).
%%%%%%%%%%%%%%%%
close all
subplotmat= 1:12;
titlemat = [1.1 1.2 1.3 1.4 2.1 2.2 2.3 2.4 3.1 3.2 3.3 3.4];
fontsize =11;
labelfontsize = 12;
axesfontsize = 12
plotline_width = 1.25;
markersize = 8;
titlefontsize = 14

rmsle_k_1 = zeros(12,1); % model 1
rmsle_k_2 = rmsle_k_1; % model 2

figure(1)
for i= 1:8
    plotNo= subplotmat(i)
    subplot(4,2,plotNo)

    hold on
    box on

    plot(networksize,k_sim(i,:),'ko','MarkerEdgeColor','k',...
    'MarkerFaceColor','k')
    hold on
    plot(networksize,k_est1(i,:),'k','LineWidth',plotline_width)
    plot(networksize,k_est2(i,:),'b','LineWidth',plotline_width)

    rmsle_k_1(i)=RMSLE(k_est1(i,:),k_sim(i,:));
    rmsle_k1 = sprintf('%0.4f ', rmsle_k_1(i))

    rmsle_k_2(i)=RMSLE(k_est2(i,:),k_sim(i,:));
    rmsle_k2 = sprintf('%0.4f ', rmsle_k_2(i))

text(61,k_est1(i,end),rmsle_k1,'FontSize',fontsize,'Color','k','FontWeight','
bold');
text(61,k_est2(i,end),rmsle_k2,'FontSize',fontsize,'Color','b','FontWeight','
bold');

xticks([0 10 20 30 40 50  60 70]);
xticklabels([0 1130 2250 3380 4510 5640 6770 7890]); % network sizes in
micron
set(gca,'fontweight','bold','fontsize',axesfontsize);
xlabel("Network size (µm)"+newline+"
",'FontSize',labelfontsize,'FontWeight','bold');
ylabel('Permeability (m^2)','FontWeight','bold', 'FontSize',labelfontsize)
```

```
xlim([0 72]);
title(['Network
',num2str(titlemat(i))],'FontSize',titlefontsize,'FontWeight','bold');

end
set(gcf, 'Units', 'centimeters');
set(gcf, 'Position', [10 0 30 80]);

figure(1)
savefig('new_k_est_v2_1.fig')
print -dtiff -r600 new_k_est_v2_1.tiff

figure(2)
for i= 9:12
    plotNo= subplotmat(i-8)
    subplot(4,2,plotNo)

    hold on
    box on

    plot(networksize,k_sim(i,:),'ko','MarkerEdgeColor','k',...
    'MarkerFaceColor','k')
    hold on
    plot(networksize,k_est1(i,:),'k','LineWidth',plotline_width)
    plot(networksize,k_est2(i,:),'b','LineWidth',plotline_width)

    rmsle_k_1(i)=RMSLE(k_est1(i,:),k_sim(i,:));
    rmsle_k1 = sprintf('%0.4f ', rmsle_k_1(i))

    rmsle_k_2(i)=RMSLE(k_est2(i,:),k_sim(i,:));
    rmsle_k2 = sprintf('%0.4f ', rmsle_k_2(i))


text(61,k_est1(i,end),rmsle_k1,'FontSize',fontsize,'Color','k','FontWeight','
bold');

text(61,k_est2(i,end),rmsle_k2,'FontSize',fontsize,'Color','b','FontWeight','
bold');

xticks([0 10 20 30 40 50  60 70]);
xticklabels([0 1130 2250 3380 4510 5640 6770 7890]); % network sizes in
micron
set(gca,'fontweight','bold','fontsize',axesfontsize);
xlabel("Network size (µm)"+newline+"
",'FontSize',labelfontsize,'FontWeight','bold');
ylabel('Permeability (m^2)','FontWeight','bold', 'FontSize',labelfontsize)
xlim([0 72]);

title(['Network
',num2str(titlemat(i))],'FontSize',titlefontsize,'FontWeight','bold');
end
set(gcf, 'Units', 'centimeters');
set(gcf, 'Position', [10 0 30 80]);

figure(2)
savefig('new_k_est_v2_2.fig')
print -dtiff -r600 new_k_est_v2_2.tiff
```

Appendix F - **Notation**

A_p	pore cross-sectional area
a_t	total current flow
A_t	medium cross-sectional area
A_w	cross-sectional area occupied by the brine
C	constant coefficient
C_{CPA}	Critical path analysis constant
D_p	pore space fractal dimension
F	formation factor
f	volume fraction
f_c	critical volume fraction
G	pore shape facto
g_h	hydraulic conductance
g_e	electrical conductance
g_{hi}	hydraulic conductance between the pore-throat interface and center of pore i
g_{hij}	hydraulic conductance between two pore bodies
g_{hj}	hydraulic conductance between the pore-throat interface and center of pore j
g_{ht}	hydraulic conductance of pore-throat
k	permeability
k_{REV}	permeability at REV point[m^2]
L	network (system) size
l_{bi}	distance in between the center of pore body to the interface where pore body and pore throat meet
l_{bj}	distance in between the center of pore body to the interface where pore body and pore throat meet
l_{ij}	distance between the centers of the two pore bodies
l_{t0}	typical pore-throat length

l_t	pore-throat length
m	empirical exponent
P_{inlet}	pressure at inlet
P_{outlet}	pressure at outlet
p	fraction of occupied or preset bonds
p_c	percolation threshold
q_{ij}	the flow rate between two pore bodies
q_t	total flow rate
R_o	resistivity of saturated medium
r_b	Pore- body radius
r_t	pore-throat radius
r_{tc}	critical pore-throat radius
r_{tmax}	maximum pore-throat radius
r_{tmin}	minimum pore-throat radius
R_w	brine resistivity
V	occupied pore volume
V_c	critical pore volume
V_s	sample volume
V_t	total volume of pores
x_{est}	estimated value
x_{sim}	simulated value
α	CPA exponent for permeability
β	CPA exponent for formation factor
γ	Weibull distributions shape parameter
ΔP_{ij}	pressure difference between two pore bodies
ΔV	voltage drop
δ	Weibull distributions shape parameter
ζ	aspect ratio for pore-body radius generation
μ	fluid viscosity
ν	correlation length scaling exponent

χ	correlation length
χ_0	typical bond length